Harmonic decomposition of three-particle azimuthal correlations at energies available at the BNL Relativistic Heavy Ion Collider

L. Adamczyk,[1] J. K. Adkins,[19] G. Agakishiev,[17] M. M. Aggarwal,[31] Z. Ahammed,[50] N. N. Ajitanand,[40] I. Alekseev,[15,26] D. M. Anderson,[42] R. Aoyama,[46] A. Aparin,[17] D. Arkhipkin,[3] E. C. Aschenauer,[3] M. U. Ashraf,[45] A. Attri,[31] G. S. Averichev,[17] X. Bai,[7] V. Bairathi,[27] A. Behera,[40] R. Bellwied,[44] A. Bhasin,[16] A. K. Bhati,[31] P. Bhattarai,[43] J. Bielcik,[10] J. Bielcikova,[11] L. C. Bland,[3] I. G. Bordyuzhin,[15] J. Bouchet,[18] J. D. Brandenburg,[36] A. V. Brandin,[26] D. Brown,[23] I. Bunzarov,[17] J. Butterworth,[36] H. Caines,[54] M. Calderón de la Barca Sánchez,[5] J. M. Campbell,[29] D. Cebra,[5] I. Chakaberia,[3] P. Chaloupka,[10] Z. Chang,[42] N. Chankova-Bunzarova,[17] A. Chatterjee,[50] S. Chattopadhyay,[50] X. Chen,[37] J. H. Chen,[39] X. Chen,[21] J. Cheng,[45] M. Cherney,[9] W. Christie,[3] G. Contin,[22] H. J. Crawford,[4] S. Das,[7] L. C. De Silva,[9] R. R. Debbe,[3] T. G. Dedovich,[17] J. Deng,[38] A. A. Derevschikov,[33] L. Didenko,[3] C. Dilks,[32] X. Dong,[22] J. L. Drachenberg,[20] J. E. Draper,[5] L. E. Dunkelberger,[6] J. C. Dunlop,[3] L. G. Efimov,[17] N. Elsey,[52] J. Engelage,[4] G. Eppley,[36] R. Esha,[6] S. Esumi,[46] O. Evdokimov,[8] J. Ewigleben,[23] O. Eyser,[3] R. Fatemi,[19] S. Fazio,[3] P. Federic,[11] P. Federicova,[10] J. Fedorisin,[17] Z. Feng,[7] P. Filip,[17] E. Finch,[47] Y. Fisyak,[3] C. E. Flores,[5] L. Fulek,[1] C. A. Gagliardi,[42] D. Garand,[34] F. Geurts,[36] A. Gibson,[49] M. Girard,[51] D. Grosnick,[49] D. S. Gunarathne,[41] Y. Guo,[18] A. Gupta,[16] S. Gupta,[16] W. Guryn,[3] A. I. Hamad,[18] A. Hamed,[42] A. Harlenderova,[10] J. W. Harris,[54] L. He,[34] S. Heppelmann,[32] S. Heppelmann,[5] A. Hirsch,[34] G. W. Hoffmann,[43] S. Horvat,[54] T. Huang,[28] B. Huang,[8] X. Huang,[45] H. Z. Huang,[6] T. J. Humanic,[29] P. Huo,[40] G. Igo,[6] W. W. Jacobs,[14] A. Jentsch,[43] J. Jia,[3,40] K. Jiang,[37] S. Jowzaee,[52] E. G. Judd,[4] S. Kabana,[18] D. Kalinkin,[14] K. Kang,[45] K. Kauder,[52] H. W. Ke,[3] D. Keane,[18] A. Kechechyan,[17] Z. Khan,[8] D. P. Kikoła,[51] I. Kisel,[12] A. Kisiel,[51] L. Kochenda,[26] M. Kocmanek,[11] T. Kollegger,[12] L. K. Kosarzewski,[51] A. F. Kraishan,[41] P. Kravtsov,[26] K. Krueger,[2] N. Kulathunga,[44] L. Kumar,[31] J. Kvapil,[10] J. H. Kwasizur,[14] R. Lacey,[40] J. M. Landgraf,[3] K. D. Landry,[6] J. Lauret,[3] A. Lebedev,[3] R. Lednicky,[17] J. H. Lee,[3] X. Li,[37] C. Li,[37] W. Li,[39] Y. Li,[45] J. Lidrych,[10] T. Lin,[14] M. A. Lisa,[29] H. Liu,[14] P. Liu,[40] Y. Liu,[42] F. Liu,[7] T. Ljubicic,[3] W. J. Llope,[52] M. Lomnitz,[22] R. S. Longacre,[3] S. Luo,[8] X. Luo,[7] G. L. Ma,[39] L. Ma,[39] Y. G. Ma,[39] R. Ma,[3] N. Magdy,[40] R. Majka,[54] D. Mallick,[27] S. Margetis,[18] C. Markert,[43] H. S. Matis,[22] K. Meehan,[5] J. C. Mei,[38] Z. W. Miller,[8] N. G. Minaev,[33] S. Mioduszewski,[42] D. Mishra,[27] S. Mizuno,[22] B. Mohanty,[27] M. M. Mondal,[13] D. A. Morozov,[33] M. K. Mustafa,[22] Md. Nasim,[6] T. K. Nayak,[50] J. M. Nelson,[4] M. Nie,[39] G. Nigmatkulov,[26] T. Niida,[52] L. V. Nogach,[33] T. Nonaka,[46] S. B. Nurushev,[33] G. Odyniec,[22] A. Ogawa,[3] K. Oh,[35] V. A. Okorokov,[26] D. Olvitt, Jr.,[41] B. S. Page,[3] R. Pak,[3] Y. Pandit,[8] Y. Panebratsev,[17] B. Pawlik,[30] H. Pei,[7] C. Perkins,[4] P. Pile,[3] J. Pluta,[51] K. Poniatowska,[51] J. Porter,[22] M. Posik,[41] A. M. Poskanzer,[22] N. K. Pruthi,[31] M. Przybycien,[1] J. Putschke,[52] H. Qiu,[34] A. Quintero,[41] S. Ramachandran,[19] R. L. Ray,[43] R. Reed,[23] M. J. Rehbein,[9] H. G. Ritter,[22] J. B. Roberts,[36] O. V. Rogachevskiy,[17] J. L. Romero,[5] J. D. Roth,[9] L. Ruan,[3] J. Rusnak,[11] O. Rusnakova,[10] N. R. Sahoo,[42] P. K. Sahu,[13] S. Salur,[22] J. Sandweiss,[54] M. Saur,[11] J. Schambach,[43] A. M. Schmah,[22] W. B. Schmidke,[3] N. Schmitz,[24] B. R. Schweid,[40] J. Seger,[9] M. Sergeeva,[6] P. Seyboth,[24] N. Shah,[39] E. Shahaliev,[17] P. V. Shanmuganathan,[23] M. Shao,[37] A. Sharma,[16] M. K. Sharma,[16] W. Q. Shen,[39] Z. Shi,[22] S. S. Shi,[7] Q. Y. Shou,[39] E. P. Sichtermann,[22] R. Sikora,[1] M. Simko,[11] S. Singha,[18] M. J. Skoby,[14] N. Smirnov,[54] D. Smirnov,[3] W. Solyst,[14] L. Song,[44] P. Sorensen,[3] H. M. Spinka,[2] B. Srivastava,[34] T. D. S. Stanislaus,[49] M. Strikhanov,[26] B. Stringfellow,[34] T. Sugiura,[46] M. Sumbera,[11] B. Summa,[32] Y. Sun,[37] X. M. Sun,[7] X. Sun,[7] B. Surrow,[41] D. N. Svirida,[15] A. H. Tang,[3] Z. Tang,[37] A. Taranenko,[26] T. Tarnowsky,[25] A. Tawfik,[53] J. Thäder,[22] J. H. Thomas,[22] A. R. Timmins,[44] D. Tlusty,[36] T. Todoroki,[3] M. Tokarev,[17] S. Trentalange,[6] R. E. Tribble,[42] P. Tribedy,[3] S. K. Tripathy,[13] B. A. Trzeciak,[10] O. D. Tsai,[6] T. Ullrich,[3] D. G. Underwood,[2] I. Upsal,[29] G. Van Buren,[3] G. van Nieuwenhuizen,[3] A. N. Vasiliev,[33] F. Videbæk,[3] S. Vokal,[17] S. A. Voloshin,[52] A. Vossen,[14] G. Wang,[6] Y. Wang,[7] F. Wang,[34] Y. Wang,[45] J. C. Webb,[3] G. Webb,[3] L. Wen,[6] G. D. Westfall,[25] H. Wieman,[22] S. W. Wissink,[14] R. Witt,[48] Y. Wu,[18] Z. G. Xiao,[45] W. Xie,[34] G. Xie,[37] J. Xu,[7] N. Xu,[22] Q. H. Xu,[38] Y. F. Xu,[39] Z. Xu,[3] Y. Yang,[28] Q. Yang,[37] C. Yang,[38] S. Yang,[3] Z. Ye,[8] Z. Ye,[8] L. Yi,[54] K. Yip,[3] I.-K. Yoo,[35] N. Yu,[7] H. Zbroszczyk,[51] W. Zha,[37] Z. Zhang,[39] X. P. Zhang,[45] J. B. Zhang,[7] S. Zhang,[37] J. Zhang,[21] Y. Zhang,[37] J. Zhang,[22] S. Zhang,[39] J. Zhao,[34] C. Zhong,[39] L. Zhou,[37] C. Zhou,[39] X. Zhu,[45] Z. Zhu,[38] and M. Zyzak[12]

(STAR Collaboration)

[1]*AGH University of Science and Technology, FPACS, Cracow 30-059, Poland*
[2]*Argonne National Laboratory, Argonne, Illinois 60439*
[3]*Brookhaven National Laboratory, Upton, New York 11973*
[4]*University of California, Berkeley, California 94720*
[5]*University of California, Davis, California 95616*
[6]*University of California, Los Angeles, California 90095*
[7]*Central China Normal University, Wuhan, Hubei 430079*
[8]*University of Illinois at Chicago, Chicago, Illinois 60607*
[9]*Creighton University, Omaha, Nebraska 68178*
[10]*Czech Technical University in Prague, FNSPE, Prague, 115 19, Czech Republic*
[11]*Nuclear Physics Institute AS CR, 250 68 Prague, Czech Republic*

[12]*Frankfurt Institute for Advanced Studies FIAS, Frankfurt 60438, Germany*
[13]*Institute of Physics, Bhubaneswar 751005, India*
[14]*Indiana University, Bloomington, Indiana 47408*
[15]*Alikhanov Institute for Theoretical and Experimental Physics, Moscow 117218, Russia*
[16]*University of Jammu, Jammu 180001, India*
[17]*Joint Institute for Nuclear Research, Dubna, 141 980, Russia*
[18]*Kent State University, Kent, Ohio 44242*
[19]*University of Kentucky, Lexington, Kentucky, 40506-0055*
[20]*Lamar University, Physics Department, Beaumont, Texas 77710*
[21]*Institute of Modern Physics, Chinese Academy of Sciences, Lanzhou, Gansu 730000*
[22]*Lawrence Berkeley National Laboratory, Berkeley, California 94720*
[23]*Lehigh University, Bethlehem, Pennsylvania 18015*
[24]*Max-Planck-Institut fur Physik, Munich 80805, Germany*
[25]*Michigan State University, East Lansing, Michigan 48824*
[26]*National Research Nuclear University MEPhI, Moscow 115409, Russia*
[27]*National Institute of Science Education and Research, Bhubaneswar 751005, India*
[28]*National Cheng Kung University, Tainan 70101*
[29]*Ohio State University, Columbus, Ohio 43210*
[30]*Institute of Nuclear Physics PAN, Cracow 31-342, Poland*
[31]*Panjab University, Chandigarh 160014, India*
[32]*Pennsylvania State University, University Park, Pennsylvania 16802*
[33]*Institute of High Energy Physics, Protvino 142281, Russia*
[34]*Purdue University, West Lafayette, Indiana 47907*
[35]*Pusan National University, Pusan 46241, Korea*
[36]*Rice University, Houston, Texas 77251*
[37]*University of Science and Technology of China, Hefei, Anhui 230026*
[38]*Shandong University, Jinan, Shandong 250100*
[39]*Shanghai Institute of Applied Physics, Chinese Academy of Sciences, Shanghai 201800*
[40]*State University Of New York, Stony Brook, New York 11794*
[41]*Temple University, Philadelphia, Pennsylvania 19122*
[42]*Texas A&M University, College Station, Texas 77843*
[43]*University of Texas, Austin, Texas 78712*
[44]*University of Houston, Houston, Texas 77204*
[45]*Tsinghua University, Beijing 100084*
[46]*University of Tsukuba, Tsukuba, Ibaraki, Japan,*
[47]*Southern Connecticut State University, New Haven, Connecticut 06515*
[48]*United States Naval Academy, Annapolis, Maryland, 21402*
[49]*Valparaiso University, Valparaiso, Indiana 46383*
[50]*Variable Energy Cyclotron Centre, Kolkata 700064, India*
[51]*Warsaw University of Technology, Warsaw 00-661, Poland*
[52]*Wayne State University, Detroit, Michigan 48201*
[53]*World Laboratory for Cosmology and Particle Physics (WLCAPP), Cairo 11571, Egypt*
[54]*Yale University, New Haven, Connecticut 06520*

(Received 24 January 2017; revised manuscript received 2 April 2018; published 28 September 2018)

We present measurements of three-particle correlations for various harmonics in Au+Au collisions at energies ranging from $\sqrt{s_{\rm NN}} = 7.7$ to 200 GeV using the STAR detector. The quantity $\langle\cos(m\phi_1 + n\phi_2 - (m+n)\phi_3)\rangle$, with ϕ being the azimuthal angles of the particles is evaluated as a function of $\sqrt{s_{\rm NN}}$, collision centrality, transverse momentum, p_T, pseudorapidity difference, $\Delta\eta$, and harmonics (m and n). These data provide detailed information on global event properties such as the three-dimensional structure of the initial overlap region, the expansion dynamics of the matter produced in the collisions, and the transport properties of the medium. A strong dependence on $\Delta\eta$ is observed for most harmonic combinations, which is consistent with breaking of longitudinal boost invariance. An interesting energy dependence is observed when one of the harmonics m, n, or $m + n$ is equal to two, for which the correlators are dominated by the two-particle correlations relative to the second-harmonic event plane. These measurements can be used to constrain models of heavy-ion collisions over a wide range of temperature and baryon chemical potential.

DOI: 10.1103/PhysRevC.98.034918

I. INTRODUCTION

Heavy nuclei are collided at facilities such as the Relativistic Heavy Ion Collider (RHIC) and the Large Hadron Collider (LHC) in order to study the emergent properties of matter with quarks and gluons as the dominant degrees of freedom: a quark-gluon plasma (QGP) [1–4]. The QGP is a form of matter that existed in the early universe when its ambient temperature was more than 155 MeV or 200 000 times hotter than the center of the sun [5,6]. As temperatures drop, quarks and gluons no longer possess the energy necessary to overcome the confining forces of QCD and they become confined into color neutral hadrons and the QGP transitions into a gas of hadrons [7]. This transition occurred in the early universe at about one microsecond after the big bang. Heavy-ion collisions provide the only known method to recreate and study that phase transition in a laboratory setting.

To provide the clearest possible picture of this phase transition, a beam energy scan was carried out at RHIC with collision energies ranging from $\sqrt{s_{\rm NN}} = 200\,{\rm GeV}$ down to 7.7 GeV. Lowering the beam energy naturally reduces the initial temperature (T) of the matter created in the collisions, as well as increases the baryon chemical potential μ_B, providing information on how the transport properties and equilibrium of the matter vary on the T and μ_B plane of the QCD phase diagram [8]. These heavy-ion collisions create systems that are both very small and short lived. The characteristic size of the collision region is the size of a nucleus or approximately 10^{-14} meter. After a collision, the system expands in the longitudinal and transverse directions so that the energy density drops quickly. Any quark gluon plasma that exists will only survive for approximately 5×10^{-23} seconds. Given the smallness of the system and its very brief lifetime, it is challenging to determine the nature of the matter left behind after the initial collisions. Physicists rely on indirect observations based on particles streaming from the collision region, which are observed long after any QGP has ceased to exist. Correlations between these produced particles have provided insight into the early phases of the expansion as well as the characteristics of the matter undergoing the expansion [9]. The dependence of the correlations on the azimuthal angle between particles $\Delta\phi = \phi_1 - \phi_2$ has proven to be particularly informative. Data have revealed that even when particle pairs are separated by large angles in the longitudinal direction (large $\Delta\eta$), they remain strongly correlated in the azimuthal direction. One example of these correlations is a prominent ridgelike structure that can be seen in the two-particle correlations; and this ridge is associated with an enhanced correlation near $\Delta\phi \sim 0$ and π and a long-range structure in $\Delta\eta$ [10].

The origin of this ridge has been traced to the initial geometry of the collision region where flux tubes are localized in the transverse direction but stretch over a long distance in the longitudinal direction [11–14]. The degree to which these structures from the initial geometry are translated into correlations between particles emitted from the collision region reveals information about the medium's viscosity. For example, larger viscosity will result in weaker correlations [15]. To study these effects, it is convenient to examine the coefficients of a Fourier transform of the $\Delta\phi$ dependence of the two-particle correlation functions [16]. These coefficients have been variously labeled as a_n or $v_n^2\{2\}$ where n is the harmonic and the quantity in curly brackets indicates a two-particle correlation. Although the latter is perhaps more cumbersome, we have maintained its usage owing to its connection to the original terminology used for two-particle cumulants, which has been in use for more than a decade [17]. The coefficients $v_n^2\{2\} = \langle \cos n(\Delta\phi)\rangle$ have previously been studied as a function of $\sqrt{s_{\rm NN}}$, centrality, harmonic n, p_T, and $\Delta\eta$ [18]. In this paper, we extend this analysis from two-particle correlations to three-particle mixed harmonic correlations of the form $\langle \cos[m\phi_1 + n\phi_2 - (m+n)\phi_3]\rangle$ [19] where m and n are positive integers.

Extending the analysis of azimuthal correlations from two to three particles provides several benefits. First, the three-particle correlations provide greater sensitivity to the three-dimensional structure of the initial state by revealing information about the two-particle $\Delta\eta - \Delta\phi$ correlations with respect to the reaction plane. Many models of heavy-ion collisions make the simplifying assumption that the initial geometry of the collision overlap does not vary with rapidity and that a boost invariant central rapidity plateau is expected [20]. It is likely, however, that this assumption is broken by the asymmetric nature of the initial state in the longitudinal direction and that precise comparisons between models and data will require a better understanding of the initial-state fluctuations in all three dimensions [21]. In addition, new measurements can constrain the model parameters [22–25]. While signals seen in two-particle correlations may be driven by multiple effects, three-particle correlations can break those ambiguities. This is important as models become more sophisticated by including bulk viscosity, shear viscosity, and their temperature dependence [26]. Also, three-particle correlations reveal information about how two-particle correlations change as a function of their angle with respect to the reaction plane. When one of the harmonics m, n, or $m+n$ is equal to two, that harmonic will be dominated by the preference of particles to be emitted in the direction of the reaction plane. This feature has been exploited to study charge separation relative to the reaction plane through measurements of the charge dependence of $\langle \cos(\phi_1 + \phi_2 - 2\phi_3)\rangle$ [27,28]. The motivation for those measurements was to search for evidence of the chiral magnetic effect (CME) in heavy-ion collisions [29–31]. By extending the measurements to other harmonics we can ascertain more information about the nature of the correlations interpreted as evidence for CME. Finally, three-particle correlations reveal information about how various harmonics are correlated with each other. For example, Teaney and Yan [22] originally proposed the measurement of $\langle \cos(\phi_1 + 2\phi_2 - 3\phi_3)\rangle$ because initial state models predict a strong correlation between the first, second and third harmonics of the spatial density distribution. That correlation can be traced to collision geometries where a nucleon from one nucleus fluctuates toward the edge of that nucleus and impinges on the oncoming nucleus. This leads to something similar to a $p + A$ collision and a high density near the edge of the main collision region. That configuration increases the predicted v_3 by a factor of 2–3 in noncentral collisions so that v_3 deviates from the $1/\sqrt{N_{\rm part}}$ dependence one would expect from random

fluctuations in the positions of the nucleons participating in the collision [15,16,18]. In analogy to a $p + A$ collision, this configuration should also be asymmetric in the forward and backward rapidity directions; again pointing to the importance of understanding the three-dimensional structure of the initial state [32–35].

In this paper we present measurements of $\langle\cos[m\phi_1 + n\phi_2 - (m+n)\phi_3]\rangle$ as a function of energy, centrality, $\Delta\eta$, p_T, and harmonics m and n. Our data confirm the correlations between the first, second, and third harmonics predicted by Teaney and Yan, but the $\Delta\eta$ dependence points to the importance of including the three-dimensional structure of the initial state in the model calculations.

Beyond the correlation of first and the third harmonics discussed above, the study of three-particle correlations is also important in understanding the hydrodynamic evolution of the system. If azimuthal correlations are dominated by hydrodynamic flow, one can expect the three-particle correlator for higher-order harmonics to be dominated by correlations of flow harmonics v_n and the corresponding event planes Ψ_n. More specifically, one can expect the approximate relations to hold $\langle\cos[m\phi_1 + n\phi_2 - (m+n)\phi_3]\rangle \sim \langle v_m v_n v_{m+n}\cos[m\Psi_m + n\Psi_n - (m+n)\Psi_{m+n}]\rangle$, for higher-order $m, n \geqslant 1$ harmonics. For harmonics $m, n = 1$, factorization breaking will lead to violation of these approximations [36]. For example, in case of $(m, n = 1, m + n = 2)$, one expects $\langle\cos(\phi_1 + \phi_2 - 2\phi_3)\rangle \sim \langle v_2\cos(\phi_1 + \phi_2 - 2\Psi_2)\rangle$, i.e., only the harmonic $m + n = 2$ associated with the third particle can be replaced by v_2 and Ψ_2 [31]. One can not express $\langle\cos(\phi_1 + \phi_2 - 2\phi_3)\rangle$ as $\langle v_1^2 v_2\cos(2\Psi_1 - 2\Psi_2)\rangle$ due to factorization breaking [36,37]. As we discuss in the following sections, these correlators provide novel ways to study the initial-state geometry [38] and nonlinear hydrodynamic response of the medium [23,24]. One important point must be noted, the event planes Ψ_n are distinct from the reaction plane $\Psi_{\rm RP}$ determined by the plane of the impact parameter and the collision direction. However, due to the almond shape of the overlap region of two nuclei in heavy-ion collisions, v_2 becomes the dominant flow coefficient and Ψ_2 may be used as a good proxy for $\Psi_{\rm RP}$. Therefore, if either of m, n, or $m + n$ is equal to two, the three-particle correlations should be dominated by two-particle correlations with respect to $\Psi_{\rm RP}$, i.e., $\langle\cos[2\phi_1 + m\phi_2 - (m+2)\phi_3]\rangle \approx \langle v_2\cos[2\Psi_{\rm RP} + m\phi_2 - (m+2)\phi_3]\rangle$. We explore these correlations in detail.

In the next section of the paper, we describe the experiment and the analysis of the data (Sec. II). We then present the results in Sec. III including the $\Delta\eta$ dependence (Sec. III A), the centrality dependence (Sec. III B), the p_T dependence (Sec. III C), and the beam energy dependence (Sec. III D). Our conclusions are presented in Sec. IV. Finally, we discuss measurements of $v_n^2\{2\}$ for $n = 1, 2, 4$, and 5 in the Appendix.

II. EXPERIMENT AND ANALYSIS

Our measurements make use of data collected from Au+Au collisions with the STAR detector at RHIC in the years 2004, 2010, 2011, 2012, and 2014. The charged particles used in this analysis are detected through their ionization energy loss in the STAR Time Projection Chamber [39]. The transverse momentum p_T, η, and charge are determined from the trajectory of the track in STAR's solenoidal magnetic field. With the 0.5 Tesla field used during data taking, particles can be reliably tracked for $p_T > 0.2$ GeV/c. The efficiency for finding particles drops quickly as p_T decreases below this value [40]. Weights have been used to correct the three-particle correlation functions for the p_T-dependent efficiency and for imperfections in the detector acceptance. The quantity analyzed and reported is

$$\begin{aligned} C_{m,n,m+n} &= \langle\cos[m\phi_1 + n\phi_2 - (m+n)\phi_3]\rangle \\ &= \left\langle\left(\frac{\sum_{i,j,k} w_i w_j w_k\cos[m\phi_i + n\phi_j - (m+n)\phi_k]}{\sum_{i,j,k} w_i w_j w_k}\right)\right\rangle, \end{aligned} \tag{1}$$

where $\langle\rangle$ represents an average over events and $\sum_{i,j,k}$ is a sum over unique particle triplets within an event. Each event is weighted by the number of unique triplets in that event. The weights $w_{i,j,k}$ are determined from the inverse of the ϕ distributions after they have been averaged over many events (which for a perfect detector should be flat) and by the p_T-dependent efficiency. The $w_{i,j,k}$ depend on the particles' p_T, η, and charge and the collisions' centrality and z-vertex location. The correction procedure is verified by checking that the ϕ distributions are flat after the correction so that $\langle\cos n(\phi)\rangle$ and $\langle\sin n(\phi)\rangle$ are near zero. With these corrections, the data represent the $C_{m,n,m+n}$ that would be seen by a detector with perfect acceptance for particles with $p_T > 0.2$ GeV/c and $|\eta| < 1$. In practice, calculating all possible combinations of three particles individually would be computationally too costly to be practical, particularly for the larger data sets at 200 GeV. In that case we use algebra based on Q vectors to reduce the computational challenge [41]. In this approach, one can avoid the three nested loops as required for sums over the three particles i, j, k in Eq. (1). One can, instead, perform a single loop over the list of particles, calculate Q_m, Q_n, Q_{m+n} and use the algebra of Ref. [41] to calculate phase space (η, p_T) integrated $C_{m,n,m+n}$ as

$$\begin{aligned} C_{m,n,m+n} = \frac{1}{N(N-1)(N-2)}(&Q_m Q_n Q^*_{m+n} - Q_m Q^*_m \\ &- Q_n Q^*_n - Q_{m+n} Q^*_{m+n} + 2), \end{aligned} \tag{2}$$

where $Q_n = \sum_j e^{in\phi_j}$ and N is the total number of particles. This is possible because for phase space integrated quantities, the three particles i, j, k are treated as indistinguishable and the information about all triplets can be contained in the complex numbers Q_m, Q_n, Q_{m+n} [41]. Differential measurements such as the $\Delta\eta$ dependence of the correlations, however, need more computations. This is because for such calculations only one particle (k) is integrated over all phase space, which can be represented by a single Q vector Q_n. The information of the two other particles (i, j) is to be determined at specific values of $\Delta\eta = \eta_i - \eta_j$, which is possible only by performing two additional nested loops. For standard mathematical formulas to express different correlators in terms of Q vectors, we refer the reader to Ref. [41].

Studying the $\Delta\eta$ dependence of the correlations also allows us to correct for the effect of track merging on the correlations. Track merging leads to a large anticorrelation between particle pairs that are close to each other in the detector. The effect becomes large in central collisions where the detector occupancy is largest. After weight corrections have been applied to correct for single-particle acceptance effects, the effect of track merging is the largest remaining correction.

We divide the data into standard centrality classes (0–5%, 5–10%, 10–20%, . . . , 70–80%) based on the number of charged hadrons within $|\eta| < 0.5$ observed for a given event. In some figures, we will report the centrality in terms of the number of participating nucleons ($N_{\rm part}$) estimated from a Monte Carlo Glauber calculations [40,42].

The three-particle correlations presented in this paper are related to the low-resolution limit of the event-plane measurements that have been explored at the LHC [43]. Corresponding results can be found by dividing $C_{m,n,m+n}$ by $\langle v_m v_n v_{m+n}\rangle$. Typically, however, v_n is measured from a two-particle correlation function such as the two-particle cumulants $v_n = \sqrt{v_n^2\{2\}}$ or a similar measurement and the $v_n^2\{2\}$ are not positive-definite quantities. As such, $\sqrt{v_n^2\{2\}}$ can, and often does, become imaginary. This is particularly true for the first harmonic and also at lower collision energies. For this reason we report the pure three-particle correlations, which, in any case, do not suffer from the ambiguities related to the low- and high-resolution limits associated with reaction-plane analyses [19,44] and are therefore easier to interpret theoretically.

III. RESULTS

In this section, we present the $\Delta\eta$ dependence of the three-particle correlations for several harmonic combinations corrected for track merging. After removing the effects of track merging and Hanbury Brown, and Twiss (HBT) correlations [45], we integrate over the $\Delta\eta$ dependence of the correlations and present the resulting integrated correlations as a function of centrality for the energies $\sqrt{s_{\rm NN}} = 200$, 62.4, 39, 27, 19.6, 14.5, 11.5, and 7.7 GeV. We also investigate the p_T dependence of the correlations by plotting them as a function of the p_T of either the first or second particle used in the correlation, i.e., the ones associated with the two lower harmonics. Finally, we study the dependence on the beam energy.

A. $\Delta\eta$ Dependence

Figure 1 shows the $\Delta\eta$ dependence of $C_{1,1,2}$ scaled by $N_{\rm part}^2$ for charged hadrons with $p_T > 0.2$ GeV/c and $|\eta| < 1$. The scaling accounts for the natural dilution of correlations expected if the more central collisions can be treated as a linear superposition of nucleon-nucleon collisions. Results for nine different centrality intervals from 200 GeV Au+Au collisions are shown. We do not include the uncertainty on $N_{\rm part}$ in our figures. The left panels show the correlations as a function of the difference in η between the first and second particle. Note that the subscripts in $C_{m,n,m+n}$ refer to the harmonic number while the subscripts for the η refers to the particle

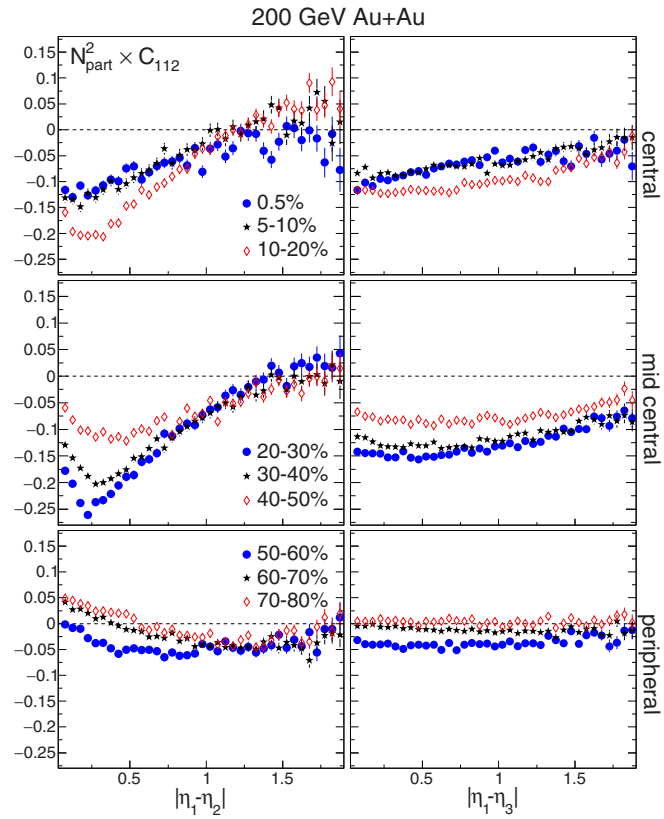

FIG. 1. The $\Delta\eta$ dependence of $C_{1,1,2}$ scaled by $N_{\rm part}^2$ for nine centrality intervals with the three most central classes shown in the top panels and the three most peripheral in the bottom. The $N_{\rm part}$ values used for the corresponding centralities are 350.6, 298.6, 234.3, 167.6, 117.1, 78.3, 49.3, 28.2, and 15.7. In the panels on the left, $\Delta\eta$ is taken between particles 1 and 2 while on the right it is between particles 1 and 3 (which is identical to 2 and 3 since $m = n = 1$ for $C_{1,1,2}$). Data are from 200 GeV Au+Au collisions and for charged hadrons with $p_T > 0.2$ GeV/c, $|\eta| < 1$.

number. The right panels show the same but as a function of the difference between particles 1 and 3. The $C_{1,1,2}$ correlation is similar to the correlation used in the search for the chiral magnetic effect except that we do not separate out the cases when particles 1 and 2 have like-sign charges vs unlike-sign charges as is done when looking for charge separation with respect to the reaction plane. These measurements can be approximately related to the reaction-plane-based measurements by scaling the three-particle correlations by $1/v_2$. We note that the difference in $C_{1,1,2}$ for different charge combinations is as large as the signal with $C_{1,1,2}$ being nearly zero for unlike-sign combinations of particle 1 and 2. This correlation may also be influenced by momentum conservation effects as well. It is not clear, however, how those effects would be distributed with respect to $\Delta\eta$.

In the left panels of Fig. 1, we see a strong dependence for $C_{1,1,2}$ on $|\eta_1 - \eta_2|$. In central collisions, the data start out negative at the smallest values of $|\eta_1 - \eta_2|$ but then begin to increase and become close to zero or even positive near $|\eta_1 - \eta_2| = 1.5$. At small $|\eta_1 - \eta_2|$, a narrow peak is seen in the correlation that is related to HBT. As we progress

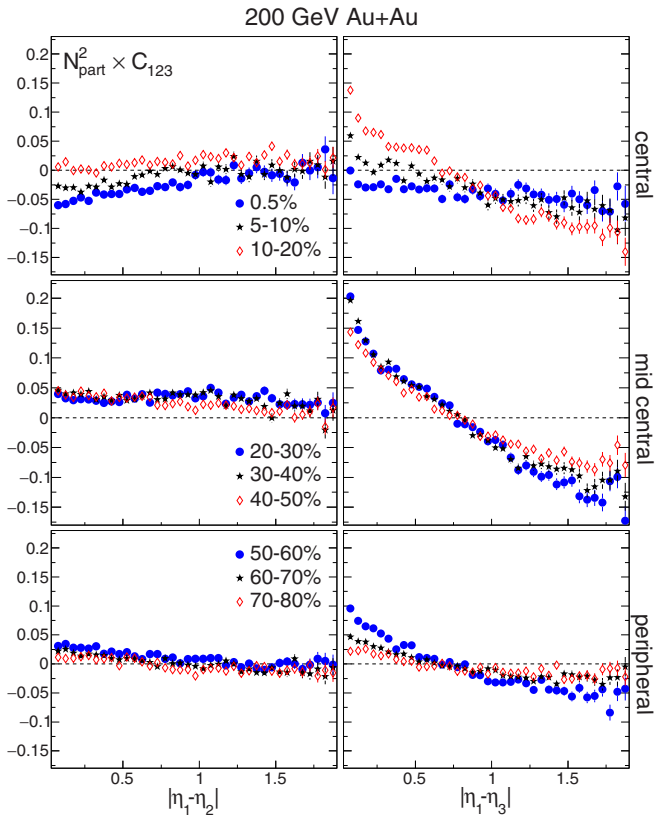

FIG. 2. The $\Delta\eta$ dependence of $C_{1,2,3}$ scaled by $N^2_{\rm part}$ for nine centrality intervals with the three most central classes shown in the top panels and the three most peripheral in the bottom. In the panels on the left, $\Delta\eta$ is taken between particles 1 and 2 while on the right it is between particles 1 and 3. Data are from 200 GeV Au+Au collisions and for charged hadrons with $p_T > 0.2$ GeV/c, $|\eta| < 1$.

from central to peripheral collisions, the trends change with $C_{1,1,2}$ in peripheral collisions exhibiting a positive value at small $|\eta_1 - \eta_2|$, perhaps signaling the dominance of jets in the correlation function in the peripheral collisions.

The left panels share the same scales as the right panels making it clear that the dependence of $C_{1,1,2}$ on $|\eta_1 - \eta_3|$ is much weaker than the dependence on $|\eta_1 - \eta_2|$. This is expected since the $e^{-2i\phi_3}$ term in $C_{1,1,2} = \langle e^{i\phi_1} e^{i\phi_2} e^{-2i\phi_3} \rangle$ will be dominated by the global preference of particles to be emitted in the direction of the reaction plane. For all but the most central collisions, the almond-shaped geometry of the collision overlap region is approximately invariant with rapidity. This is not likely the case for other harmonics [32–35]. For example, in Ref. [34] it was demonstrated using AMPT calculations that in typical midcentral heavy-ion collisions, the longitudinal decorrelation of the second-order flow harmonics is about 2–3%, whereas for the third-order harmonics it is about 15%, over two units of rapidity.

Figure 2 shows $C_{1,2,3}$ scaled by $N^2_{\rm part}$ as a function of $|\eta_1 - \eta_2|$ (left panels) and $|\eta_1 - \eta_3|$ (right panels). In this case, $C_{1,2,3}$ exhibits a stronger dependence on $|\eta_1 - \eta_3|$ than on $|\eta_1 - \eta_2|$. The dependence (both magnitude and variation) of $C_{1,2,3}$ with $|\eta_2 - \eta_3|$ is very similar to the dependence with $|\eta_1 - \eta_2|$ and is omitted from the figures to improve legibility. Again, the $e^{i2\phi_2}$ component of $C_{1,2,3}$ is dominated by the reaction plane, which is largely invariant within the η range covered by these measurements so that $C_{1,2,3}$ depends very little on the η_2, $|\eta_1 - \eta_2|$, or $|\eta_2 - \eta_3|$. However, $C_{1,2,3}$ depends very strongly on $|\eta_1 - \eta_3|$. This dependence may arise from the longitudinal asymmetry inherent in the fluctuations that lead to predictions for large values of $C_{1,2,3}$ [24]. Aforementioned, in models for the initial geometry, the correlations are induced between the first, second, and third harmonics of the eccentricity by cases where a nucleon fluctuates towards the edge of the nucleus [46]. If that occurs in the reaction-plane direction and towards the other nucleus in the collision, then that nucleon can collide with many nucleons from the other nucleus. This geometry will cause the first and third harmonics to become correlated with the second harmonic. Since the collision of one nucleon from one nucleus with many nucleons in the other nucleus is asymmetric along the rapidity axis, we argue that we can expect a strong dependence on $|\eta_1 - \eta_3|$. Models that assume the initial energy density is symmetric with rapidity (boost invariant) will likely fail to describe this behavior. One may also speculate that the variation with $|\eta_1 - \eta_3|$ could arise from sources such as jets or resonances particularly if they interact with the medium so that they become correlated with the reaction plane. Making use of the full suite of measurements provided here will help discriminate between these two scenarios.

In Fig. 3, we present the $|\eta_1 - \eta_2|$ and $|\eta_1 - \eta_3|$ dependence of $C_{2,2,4}$. This correlation is more strongly influenced by the reaction-plane correlations and exhibits much larger values than either $C_{1,1,2}$ or $C_{1,2,3}$. The dependence on $|\eta_1 - \eta_2|$ and $|\eta_1 - \eta_3|$ are also weaker with $C_{2,2,4}$ in central and midcentral collisions showing little variation over the $|\eta_1 - \eta_2|$ range, consistent with a mostly η-independent reaction plane within the measured range. A larger variation is observed with $|\eta_1 - \eta_3|$, which in midcentral collisions amounts to an approximately 20% variation. We also note that in midcentral collisions, the change in value of $C_{2,2,4}$ over the range $0 < |\eta_1 - \eta_3| < 2$ is similar in magnitude to the change of $C_{1,1,2}$ over $0 < |\eta_1 - \eta_2| < 2$ and $C_{1,2,3}$ over $0 < |\eta_1 - \eta_3| < 2$.

In Fig. 4, we present the $|\eta_1 - \eta_2|$ and $|\eta_2 - \eta_3|$ dependence of $C_{2,3,5}$. Again, $C_{2,3,5}$ only exhibits a weak dependence on $|\eta_1 - \eta_2|$ but a stronger dependence on $|\eta_2 - \eta_3|$. The dependence of $C_{2,3,5}$ with $|\eta_1 - \eta_3|$ is found to be very similar to that with $|\eta_1 - \eta_2|$, we have therefore omitted it from the figures. In central and midcentral collisions, a strong short-range correlation peak at $|\eta_2 - \eta_3| < 0.4$ is observed; it is consistent with HBT and Coulomb correlations that vary with respect to the reaction plane. In addition to that peak, $C_{2,3,5}$ decreases as $|\eta_2 - \eta_3|$ increases. Although the relative variation of $C_{2,3,5}$ is similar to $C_{2,2,4}$, the change in magnitude is much smaller than for $C_{1,1,2}$, $C_{1,2,3}$, or $C_{2,2,4}$.

The combination of the various $C_{m,n,m+n}$ can help elucidate the nature of the three-particle correlations. If the $|\eta_1 - \eta_3|$ dependence of $C_{1,2,3}$ arises from correlations between particles from jets correlated with the reaction plane, we would expect the particles at small $\Delta\eta$ to predominantly come from the near-side jet (at $\Delta\phi \approx 0$) and particles at larger $\Delta\eta$ to come from the away-side jet (at $\Delta\phi \approx \pi$ radians). In that

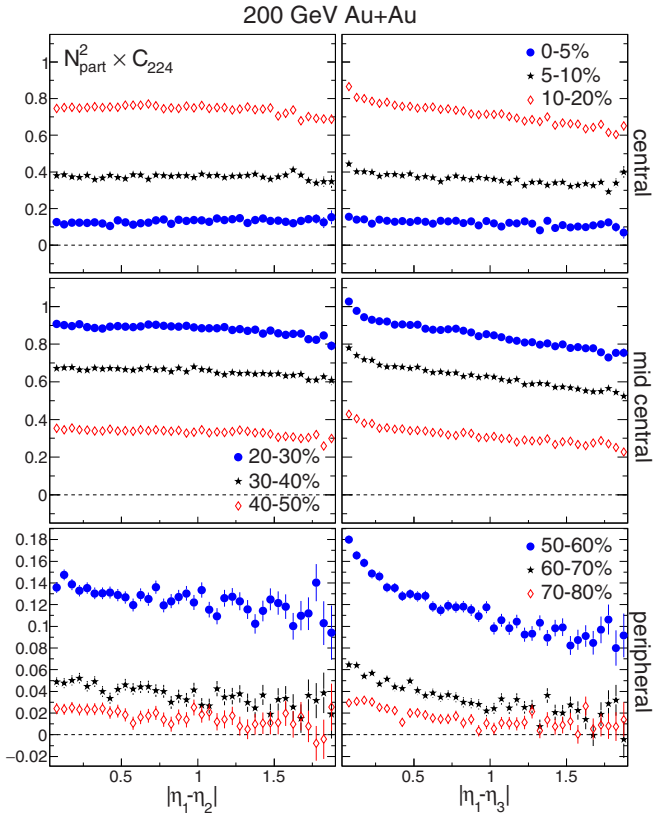

FIG. 3. The $\Delta\eta$ dependence of $C_{2,2,4}$ scaled by $N^2_{\rm part}$ for nine centrality intervals with the three most central classes shown in the top panels and the three most peripheral in the bottom. In the panels on the left, $\Delta\eta$ is taken between particles 1 and 2 while on the right it is between particles 1 and 3 (which is identical to 2 and 3 since $m = n = 2$ for $C_{2,2,4}$). Data are from 200 GeV Au+Au collisions and for charged hadrons with $p_T > 0.2$ GeV/c, $|\eta| < 1$.

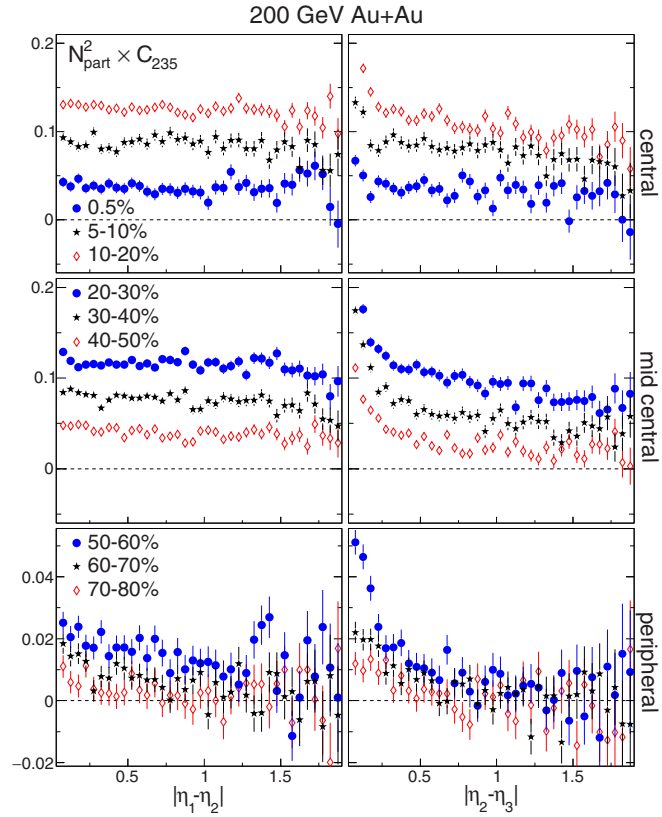

FIG. 4. The $\Delta\eta$ dependence of $C_{2,3,5}$ scaled by $N^2_{\rm part}$ for nine centrality intervals with the three most central classes shown in the top panels and the three most peripheral in the bottom. In the panels on the left, $\Delta\eta$ is taken between particles 1 and 2 while on the right it is between particles 2 and 3. Data are from 200 GeV Au+Au collisions and for charged hadrons with $p_T > 0.2$ GeV/c, $|\eta| < 1$.

case, at small $\Delta\eta$, $C_{m,n,m+n}$ for all harmonics will have a positive contribution from the jets. The same is not true, however, for large $\Delta\eta$ where we would expect the correlations to be dominated by the away-side jet separated by π radians. For this case at large $\Delta\eta$, $C_{1,1,2}$, and $C_{1,2,3}$ would receive negative contributions from the away side jet while $C_{2,2,4}$ and $C_{2,3,5}$ would both receive positive contributions. The trends observed across the variety of $C_{m,n,m+n}$ measurements are inconsistent with this simple picture with $C_{2,2,4}$ decreasing by nearly the same amount as $C_{1,2,3}$ as $\Delta\eta$ is increased. A more complicated picture of the effect of jets would therefore be required to account for the observed data but it appears difficult to construct a non-flow scenario that can account for the long-range variation of $C_{m,n,m+n}$. Breaking of boost invariance in the initial density distributions may provide an explanation for the observed variations but we do not know of any specific model that has been shown to describe our data.

B. Centrality dependence

In Figs. 5 and 6 we show $C_{m,n,m+n}$ correlations scaled by $N^2_{\rm part}$ with $(m, n) = (1, 1)$, (1,2), (1,3), (2,2), (2,3), (2,4), (3,3), and (3,4) for $\sqrt{s_{\rm NN}} = 200$, 62.4, 39, 27, 19.6, 14.5, 11.5, and 7.7 GeV Au+Au collisions as a function of $N_{\rm part}$. Data are for charged particles with $|\eta| < 1$ and $p_T > 0.2$ GeV/c. The correlation $C_{2,2,4}$, by far the largest of the measured correlations, has been scaled by a factor of 1/5. Otherwise, the scales on each of the three panels are kept the same for each energy to make it easier to compare the magnitudes of the different harmonic combinations.

At 200 GeV, $C_{1,1,2}$ is negative for all centralities except for the most peripheral where it is slightly positive but consistent with zero. $C_{1,2,3}$ is consistent with zero in peripheral collisions, positive in midcentral collisions, but then becomes negative in central collisions. If the second and third harmonic event planes are uncorrelated, then $C_{1,2,3}$ should be zero. The $C_{1,2,3}$ correlation is nonzero deviating from that expectation. The magnitude is, however, much smaller than originally anticipated based on a linear hydrodynamic response to initial-state geometry fluctuations [22]. Nonlinear coupling between harmonics, where the fifth harmonic, for example, is dominated by a combination of the second and third harmonic, has been shown to be very important [23,47]. In the case of $C_{1,2,3}$, the nonlinear contribution has an opposite sign to the linear contribution and similar magnitude canceling out most of the expected strength of $C_{1,2,3}$. This suggests that $C_{1,2,3}$ is very sensitive to the nonlinear nature of the hydrodynamic

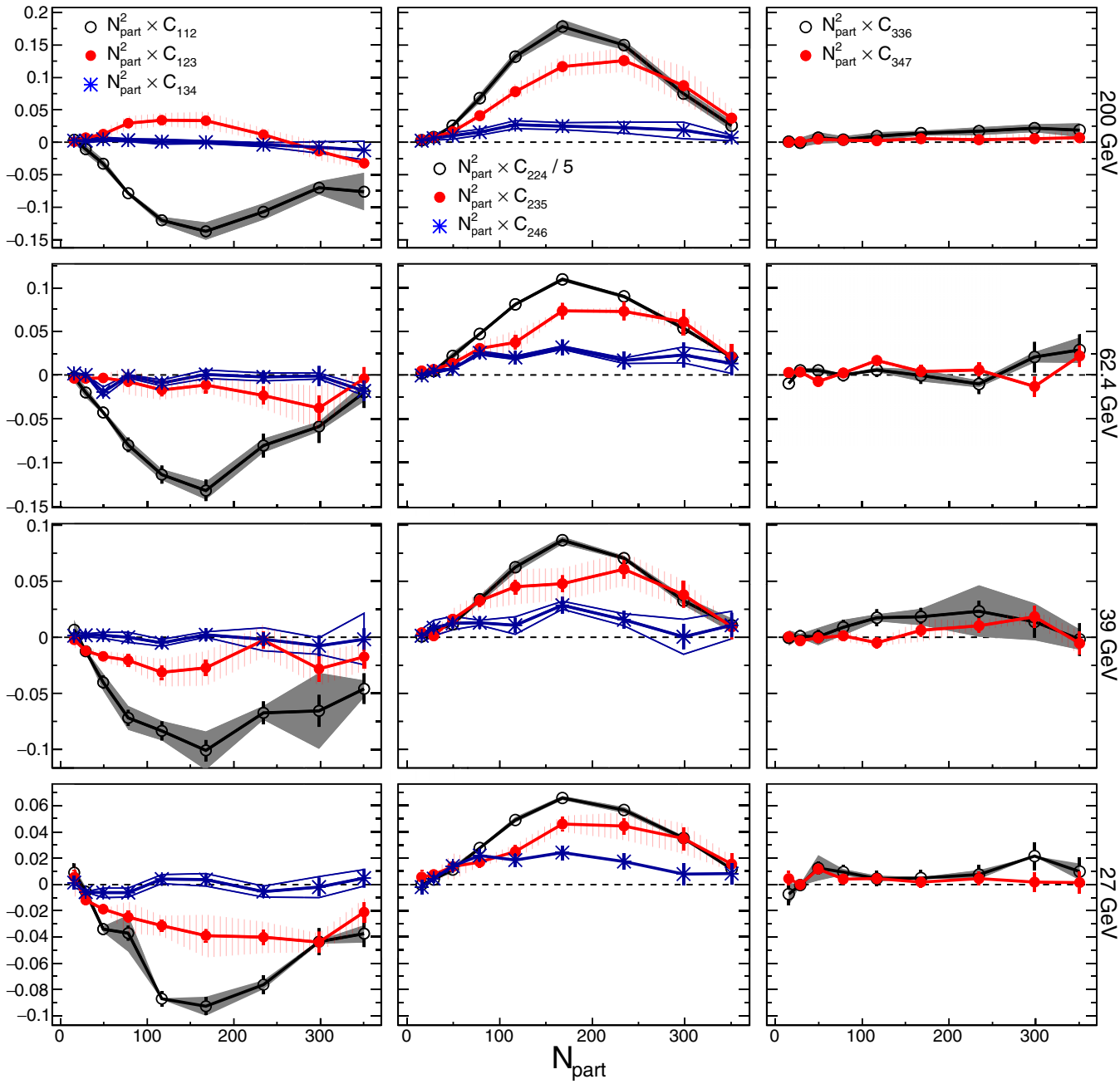

FIG. 5. The centrality dependence of the $C_{m,n,m+n}$ correlations scaled by N^2_{part} for charged hadrons with $p_T > 0.2$ GeV/c and $|\eta| < 1$ from 200, 62.4, 39, and 27 GeV Au+Au collisions for $(m, n) = (1, 1)$, $(1, 2)$, $(1, 3)$ (left), $(2, 2)$, $(2, 3)$, $(2, 4)$ (center), and $(3, 3)$, $(3, 4)$ (right). Systematic errors are shown as bands. All panels in the same row share the same scale but $C_{2,2,4}$ has been divided by a factor of 5 to fit on the panel. The labels in the top panels apply to all the panels in same column.

model. $C_{1,3,4}$ is close to zero for all centralities indicating little or no correlation between the first, third, and fourth harmonics. The other $C_{m,n,m+n}$ correlations are positive for all centralities. When considering the comparison of these data to hydrodynamic models, it is important to also consider the strong $\Delta\eta$ dependence of the correlations as shown in the previous section.

The correlations involving a second harmonic are largest with $C_{2,2,4}$ being approximately five times larger in magnitude than the next largest correlator $C_{2,3,5}$. The correlations decrease quickly as harmonics are increased beyond $n = 2$. The higher harmonic correlations $C_{3,3,6}$ and $C_{3,4,7}$ are both small but nonzero. The correlations $C_{1,1,2}$, $C_{1,2,3}$, $C_{2,2,4}$, $C_{2,3,5}$, and $C_{3,3,6}$ scaled by N^2_{part} all exhibit extrema in midcentral collisions where the initial overlap geometry is predominantly elliptical. We note that the centrality at which $N^2_{\text{part}}C_{2,2,4}$ reaches a maximum is different than the centrality at which $N^2_{\text{part}}C_{2,3,5}$ reaches a maximum.

As the collision energy is reduced, the centrality dependence and ordering of the different correlators remain mostly

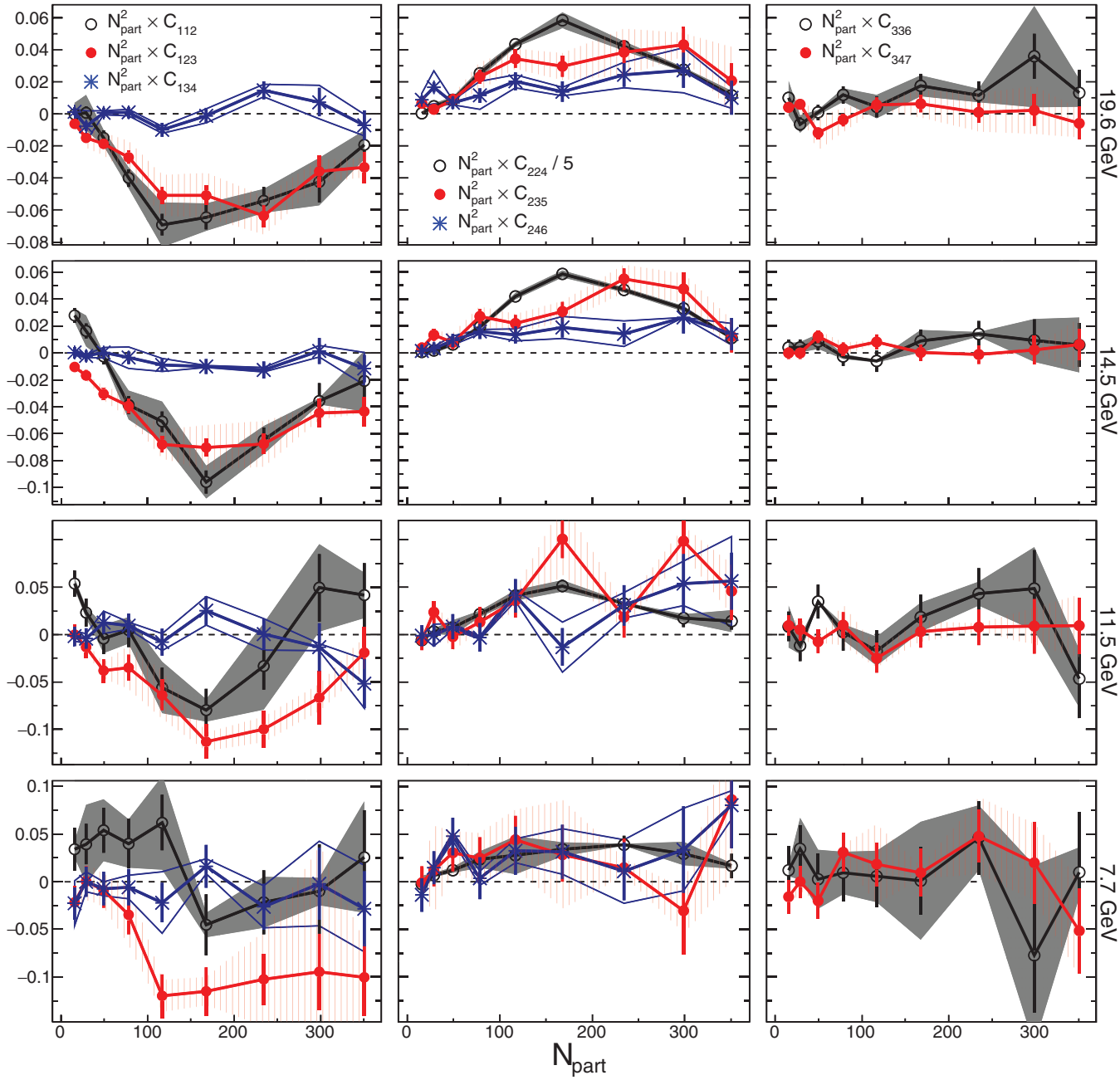

FIG. 6. The same quantities as Fig. 5 but for the lower energy Au+Au collisions 19.6, 14.5, 11.5, and 7.7 GeV.

the same although their magnitude becomes smaller. The $C_{1,2,3}$ correlation, however, is an exception.

It is mostly positive at 200 GeV but at 62.4 GeV it is consistent with zero or slightly negative. At lower energies $C_{1,2,3}$ becomes more and more negative. We speculate that this behavior may be related to the increasing importance of momentum conservation as the number of particles produced in the collision decreases although no theoretical guidance exists for the energy dependence of these correlations at energies below 200 GeV. In the future, these data will provide useful constraints for models being developed to describe low-energy collisions associated with the energy scan program at RHIC.

Figure 6 shows the same correlations as Fig. 5 except for lower-energy data sets: $\sqrt{s_{\rm NN}} = 19.6$, 14.5, 11.5, and 7.7 GeV. Trends similar to those seen in Fig. 5 are for the most part also exhibited in this figure. A second phase of the RHIC beam energy scan planned for 2019 and 2020 will significantly increase the number of events available for analysis at these lower energies while expanding the η acceptance from $|\eta| < 1$ to $|\eta| < 1.5$ [48] so that this intriguing observation can be further investigated. The increased acceptance will increase the number of three-particle combinations by approximately a factor of three and will make it possible to measure the $\Delta\eta$ dependence of the $C_{m,n,m+n}$ correlations to $|\Delta\eta| \approx 3$.

C. p_T Dependence

If the three-particle correlations presented here are dominated by correlations between event planes, then one might expect that the p_T dependence of the three-particle correlations will simply track the p_T dependence of the relevant v_n [22]:

$$\langle \cos[m\phi_1(p_T) + n\phi_2 - (m+n)\phi_3] \rangle \approx \frac{v_m(p_T)}{\varepsilon_m} \frac{v_n}{\varepsilon_n} \frac{v_{m+n}}{\varepsilon_{m+n}} \times \langle \varepsilon_m \varepsilon_n \varepsilon_{m+n} \cos[m\Psi_m + n\Psi_n - (m+n)\Psi_{m+n}] \rangle, \quad (3)$$

where ε_m is the mth harmonic eccentricity and Ψ_m is the mth harmonic participant plane angle. For the purpose of simplicity in this paper, we have scaled the correlations by $N^2_{\rm part}/p_T$ to account for the general increase of $v_n(p_T)$ with p_T [49]. That simple scaling is only valid at lower p_T and for $n \neq 1$. It does, however, aid in visualizing trends in the data, which would otherwise be visually dominated by the larger p_T range. Our primary reason for introducing Eq. (3) is to provide a context for understanding the p_T dependence of $C_{m,n,m+n}$. The relationship between $C_{m,n,m+n}$ and harmonic planes in Eq. (3) is not guaranteed to hold and is particularly likely to be broken for correlations involving the first harmonic where momentum conservation effects will likely play an important role [36] or where a strong charge sign dependence has been observed [27,28].

In Fig. 7, we show $N^2_{\rm part}C_{1,1,2}/p_T$ as a function of the p_T of particle one. The top panel shows the more central collisions while the bottom panel shows more peripheral collisions. In this and in the following figures related to the p_T dependence, we sometimes exclude centrality bins and slightly shift the positions of the points along the p_T axis to make the figures more readable. For more central collisions, $C_{1,1,2}/p_{T,1}$ is negative and slowly decreases in magnitude as $p_{T,1}$ increases. This indicates that $C_{1,1,2}$ is generally increasing with the p_T of particle one but that for central collisions at high p_T, $C_{1,1,2}$ starts to saturate. For the more peripheral 30–40% and 40–50% collision, however, $C_{1,1,2}$ appears to be linear in p_T without an indication of saturation even up to $p_T \approx 10$ GeV/c. For the much more peripheral 60–70% and 70–80% centrality intervals, $C_{1,1,2}$ starts out at or above zero then becomes more and more negative as p_T is increased. The trends in the most peripheral centrality intervals, particularly at high p_T, are consistent with being dominated by momentum conservation and jets. A pair of back-to-back particles aligned with the reaction plane will lead to a negative value for $C_{1,1,2}$. Although the data exhibit a smooth transition from the trends in more central collisions to the trends in more peripheral collisions, the trends are quite distinct and indicative of very different correlations in those different regions. In peripheral collisions, the correlations get stronger as p_T is increased. In central collisions, the opposite is observed.

For the case of $C_{1,2,3}$ in Fig. 8, we show the p_T dependence of both particle one (left panels) and particle two (right panels). The dependence of $C_{1,2,3}/p_{T,2}$ on $p_{T,2}$ is quite weak indicating that where $C_{1,2,3}$ is nonzero, it increases roughly

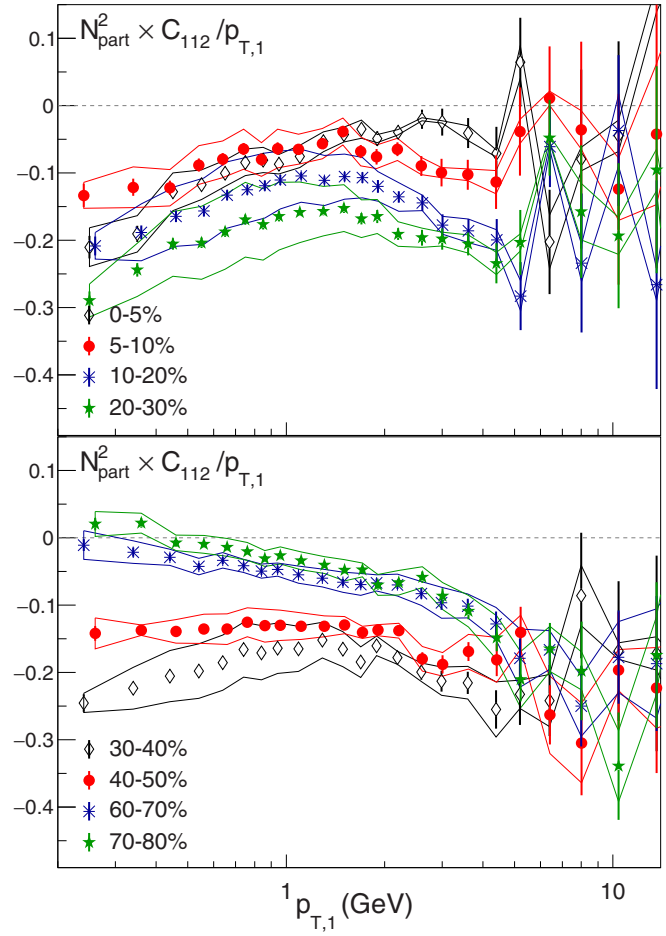

FIG. 7. Three-particle azimuthal correlations $C_{1,1,2}$ scaled by $N^2_{\rm part}/p_{T,1}$ as a function of the first particles p_T for 200 GeV Au+Au collisions for charged hadrons with $p_T > 0.2$ GeV/c and $|\eta| < 1$. The top and bottom panels show the same quantity but for a different set of centrality intervals. Systematic errors are shown as solid lines enclosing the respective data points.

linearly with $p_{T,2}$. The dependence of $C_{1,2,3}/p_{T,1}$ on $p_{T,1}$, however, exhibits several notable trends. First we note that for the 20–30% centrality interval, $C_{1,2,3}/p_{T,1}$ changes sign up to three times. In hydrodynamic models, the value of $C_{1,2,3}$ is very sensitive to the interplay between linear and nonlinear effects and to viscous effects [22]. The sign oscillations exhibited in the data may be a consequence of subtle changes in the relevant sizes of those effects. If this is the case, then this confirms that $C_{1,2,3}$ is a powerful measurement to help tune those models. At intermediate $p_{T,1}$ (2–5 GeV/c), $C_{1,2,3}$ is positive for central collisions but negative for peripheral collisions. At $p_T > 7$ GeV/c, $C_{1,2,3}$ is strongly negative, perhaps again indicative of the contribution of back-to-back jets to the correlations. Strong negative correlations are absent in central collisions where $C_{1,2,3}$ appears to remain positive, although with large error bars. This is consistent with a scenario where dijets have been quenched in central collisions. As with $C_{1,1,2}$, the p_T trends for $C_{1,2,3}$ are very different in the most peripheral and most central collisions.

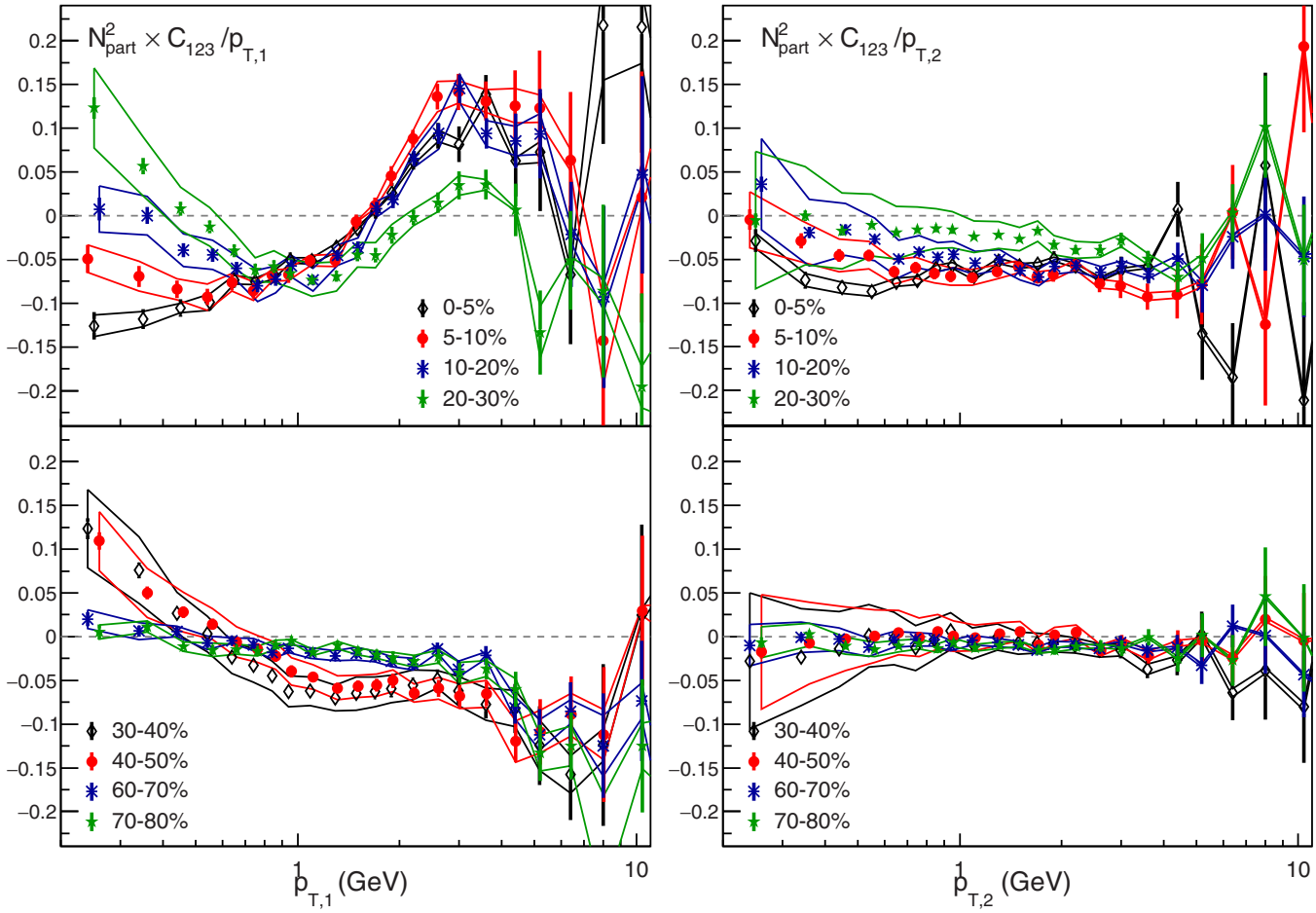

FIG. 8. Three-particle azimuthal correlations $C_{1,2,3}$ scaled by N^2_{part}/p_T as a function of the p_T using the p_T of particle one (left panels) or of particle two (right panels) for 200 GeV Au+Au collisions. Data are for charged hadrons with $p_T > 0.2$ GeV/c and $|\eta| < 1$. The top and bottom panels show the same quantity but for a different set of centrality intervals. Systematic errors are shown as solid lines enclosing the respective data points.

The $C_{2,2,4}$ correlation is the largest of the $C_{m,n,m+n}$ correlations. In Fig. 9, we show $N^2_{\text{part}} C_{2,2,4}/p_{T,1}$ as a function of $p_{T,1}$. At low $p_{T,1}$, the centrality dependence of the correlations is as expected from Fig. 5 (top panels) where we saw that the integrated value of $N^2_{\text{part}} C_{2,2,4}$ is largest for midcentral collisions. This is a natural consequence of the fact that the initial second harmonic eccentricity decreases as collisions become more central while the efficiency of converting that eccentricity into momentum-space correlations increases (with multiplicity). The competition of these two trends leads to a maximum for second harmonic correlations in midcentral collisions. This well-known [49] and generic trend does not persist to higher values of $p_{T,1}$. We see a clear change in trends at $p_{T,1} > 5$ GeV/c with the most peripheral collisions having the largest correlation strength while $N^2_{\text{part}} C_{2,2,4}/p_{T,1}$ drops significantly as a function of $p_{T,1}$ for the midcentral collisions. We note that past measurements of p_T spectra and $v_2(p_T)$ for identified particles have indicated that the effects of flow may persist up to 5 or 6 GeV/c [49]. This observation is consistent with model calculations that show in a parton cascade even up to $p_T \approx 5$ GeV/c there are a significant number of partons whose final momenta have been increased by interactions with the medium [50]. The $p_{T,1}$ dependence of $C_{2,2,4}/p_{T,1}$ supports that picture as well.

In Fig. 10, we show the p_T dependence of $N^2_{\text{part}} C_{2,3,5}/p_T$ where p_T is either the p_T of particle one (left panels) or particle two (right panels). Again, the top panels show more central collisions and the bottom panels more peripheral. For $p_T < 5$, $C_{2,3,5}/p_T$ is mostly flat as a function of the p_T of either particle one or particle two. Above that, the correlations seem to become smaller but with large statistical errors. One can discern a slight difference between the trends in the left and right panels: $C_{2,3,5}/p_{T,1}$ seems to decrease slightly as a function of $p_{T,1}$, while $C_{2,3,5}/p_{T,2}$ as a function of $p_{T,2}$ seems to increase slightly. This is likely related to the different p_T dependences of v_2 and v_3 where v_2 has been found to saturate at lower p_T while v_3 is still growing. In central collisions, it is even found that v_3 becomes larger than v_2 at intermediate p_T [16].

We have tried to point out interesting features in the p_T dependence of the correlations. In particular, we note that the p_T trends are very different when comparing central collisions to peripheral collisions. We expect that when these data are compared to model calculations, they will provide even greater insights into the interplay between the effects of

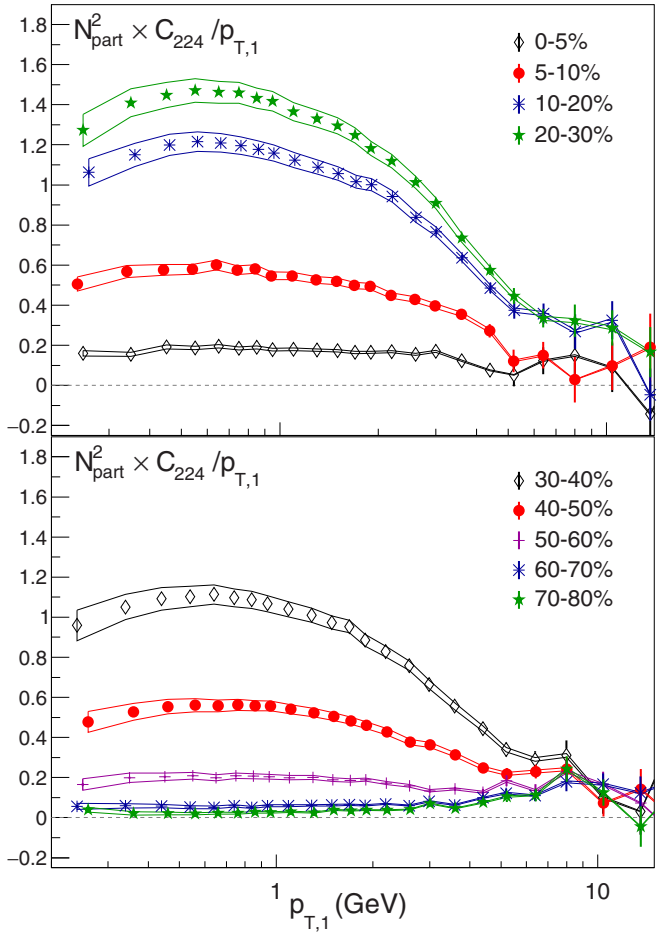

FIG. 9. Three-particle azimuthal correlations $C_{2,2,4}$ scaled by $N^2_{\rm part}/p_{T,1}$ as a function of $p_{T,1}$ for 200 GeV Au+Au collisions. Data are for charged hadrons with $p_T > 0.2$ GeV/c and $|\eta| < 1$. The top and bottom panels show the same quantity but for a different set of centrality intervals. Systematic errors are shown as solid lines enclosing the respective data points.

hard scattering, shear viscosity, bulk viscosity, the collision lifetime, and nonlinear couplings between harmonics.

D. Energy dependence

While Figs. 5 and 6 show the centrality dependence of eight different $C_{m,n,m+n}$ correlations for eight beam energies, in this section we will investigate the energy dependence in greater detail by showing the centrality dependence of individual $C_{m,n,m+n}$ correlations for a variety of energies. We will then show correlations at specific centrality intervals as a function of $\sqrt{s_{\rm NN}}$ scaled by v_2. Finally we will discuss implications of the energy dependence of the correlations.

Figure 11 shows the centrality dependence of $N^2_{\rm part}C_{1,1,2}$ (left) and $N^2_{\rm part}C_{1,2,3}$ (right) for 200, 62.4, 27, 14.5, and 7.7 or 11.5 GeV collisions. Some energies are omitted for clarity. For $N^2_{\rm part}C_{1,1,2}$, the general centrality trend appears to remain the same at all energies except 7.7 GeV, even though the magnitude slightly decreases. For midcentral collisions, $C_{1,1,2}$ is negative for all the energies shown. The 7.7 GeV data may deviate from the trend observed for the other energies as will be discussed later. For $N^2_{\rm part}C_{1,2,3}$, the energy dependence is quite different. The only positive values for $C_{1,2,3}$ are for 200 GeV collisions. At 62.4 GeV, $N^2_{\rm part}C_{1,2,3}$ has a slightly negative value that is within errors, independent of centrality. As the energy decreases, $C_{1,2,3}$ becomes more negative so that the centrality dependence of $C_{1,2,3}$ at 14.5 GeV is nearly the mirror reflection of the 200 GeV data. As will be discussed below, the change in sign of $C_{1,2,3}$ has interesting implications for how two-particle correlations relative to the reaction-plane change as a function of beam energy.

Figure 12 shows the centrality dependence of $N^2_{\rm part}C_{2,2,4}$ and $N^2_{\rm part}C_{2,3,5}$ for a selection of collision energies. Both $C_{2,2,4}$ and $C_{2,3,5}$ remain positive for the centralities and energies shown with no apparent changes in the centrality trends. We note that although $C_{2,2,4}$ drops significantly from 200 down to 19.6 GeV, we observe little change with energy below 19.6 GeV. A similar lack of energy dependence between 7.7 and 19.6 GeV was also observed in recent measurements of $v_3^2\{2\}$ [18]. This is notable since one would naively expect either of these correlation measurements to continuously increase as the density of the collision region increases.

To better view the energy trends, in Fig. 13, we show $N_{\rm part}C_{m,n,m+n}/v_2$ as a function of $\sqrt{s_{\rm NN}}$ for three centrality intervals: 10–20%, 20–30%, and 30–40%. The v_2 values are based on a two-particle cumulant analysis as discussed in Appendix A. The scaling will be further discussed in the next paragraph. For all centrality intervals shown, $C_{1,1,2}/v_2$ is negative at the highest energy but the magnitude of the correlation decreases as the energy decreases and becomes consistent with zero, although with large errors, at 7.7 GeV. This behavior was also observed in the charge dependence of this correlator, which has been studied to search for the charge separation predicted to be a consequence of the chiral magnetic effect [51]. As noted above, both $C_{2,2,4}$ and $C_{2,3,5}$ are positive for all energies. The energy dependence of $C_{1,2,3}/v_2$ is unique in that it is positive at 200 GeV but then drops below zero near 62.4 GeV and continues to become more negative at lower energies.

The correlations $C_{1,1,2}$, $C_{1,2,3}$, $C_{2,2,4}$, and $C_{2,3,5}$ presented in Fig. 13 have either $m = 2$, $n = 2$, or $m + n = 2$. When v_2 is large, as it is for the 10–20%, 20–30%, and 30–40% centrality intervals, then $\langle\cos(1\phi_1 + 1\phi_2 - 2\phi_3)\rangle/v_2 \approx \langle\cos(1\phi_1 + 1\phi_2 - 2\Psi_{\rm RP})\rangle$ and $\langle\cos[2\phi_1 + m\phi_2 - (m+2)\phi_3]\rangle/v_2 \approx \langle\cos[2\Psi_{\rm RP} + m\phi_2 - (m+2)\phi_3]\rangle$ where $\Psi_{\rm RP}$ is the reaction-plane angle. Correlations including a second harmonic should then provide information about two-particle correlations with respect to the second harmonic reaction plane:

$$\begin{aligned}
\langle\cos(1\phi_1 + 1\phi_3 - 2\phi_2)\rangle/v_2 &\approx \langle\cos(1\phi_1' + 1\phi_2')\rangle,\\
\langle\cos(1\phi_1 + 2\phi_3 - 3\phi_2)\rangle/v_2 &\approx \langle\cos(1\phi_1' - 3\phi_2')\rangle,\\
\langle\cos(2\phi_1 + 2\phi_3 - 4\phi_2)\rangle/v_2 &\approx \langle\cos(2\phi_1' - 4\phi_2')\rangle,\\
\langle\cos(2\phi_3 + 3\phi_1 - 5\phi_2)\rangle/v_2 &\approx \langle\cos(3\phi_1' - 5\phi_2')\rangle,
\end{aligned} \tag{4}$$

where $\phi' = \phi - \Psi_{\rm RP}$. Since we are integrating over all particles in these correlations, the subscript label for the particles is arbitrary so we have reassigned them so that particle three is always associated with the second harmonic. For illustration,

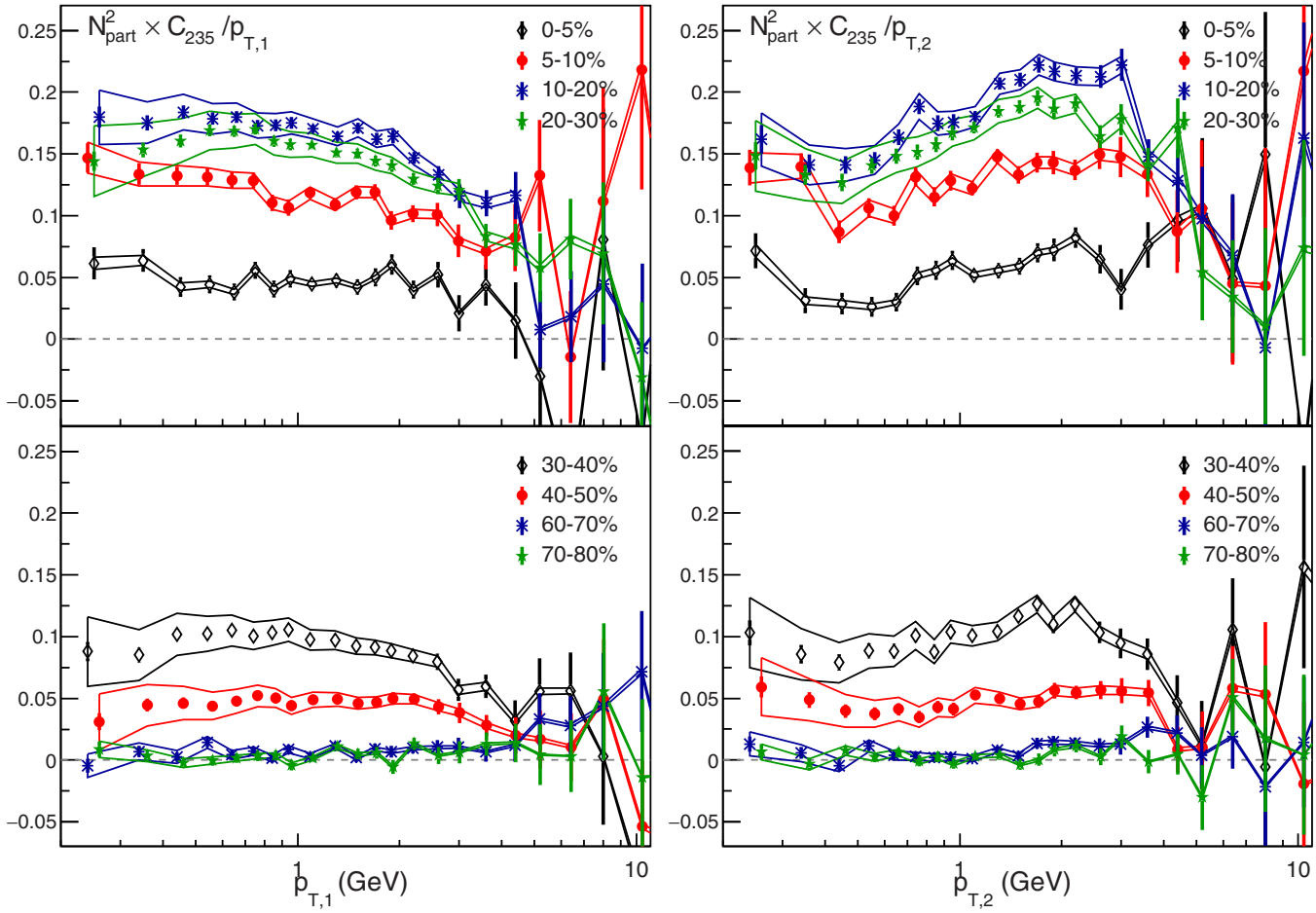

FIG. 10. Three-particle azimuthal correlations $C_{2,3,5}$ scaled by $N^2_{\rm part}/p_T$ as a function of p_T where the p_T is taken for either particle one (left panels) or particle two (right panels) for 200 GeV Au+Au collisions. Data are for charged hadrons with $p_T > 0.2$ GeV/c and $|\eta| < 1$. The top and bottom panels show the same quantity but for a different set of centrality intervals. Systematic errors are shown as solid lines enclosing the respective data points.

Table I shows values for $C_{m,n,m+n}/v_2$ for specific values of ϕ_1' and ϕ_2'. At 200 GeV, all measured correlations are positive except $\langle\cos(\phi_1' + \phi_2')\rangle$. This points to an enhanced probability for a pair of particles in one of two possible configurations: either $\phi_1' \approx \pi/3$ and $\phi_2' \approx 2\pi/3$ or $\phi_1' \approx -\pi/3$ and $\phi_2' \approx -2\pi/3$ (these correspond to the rightmost column of Table I). This result is surprising since it implies a preference for both of the correlated particles to either be in the upper hemisphere, or both in the lower hemisphere. We note, however, that hydrodynamic models with fluctuating initial conditions correctly predict this trend [52], which could arise from increased density fluctuations at either the top or the bottom of the

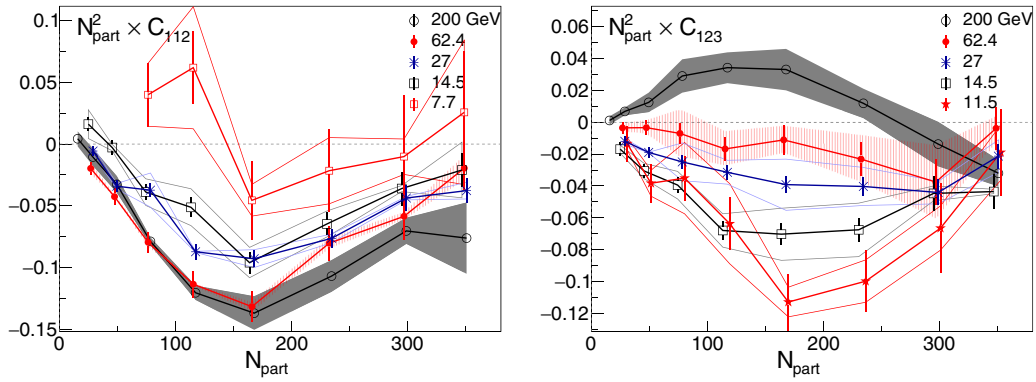

FIG. 11. The centrality dependence of $C_{1,1,2}$ (left) and $C_{1,2,3}$ (right) scaled by $N^2_{\rm part}$ for a selection of energies.

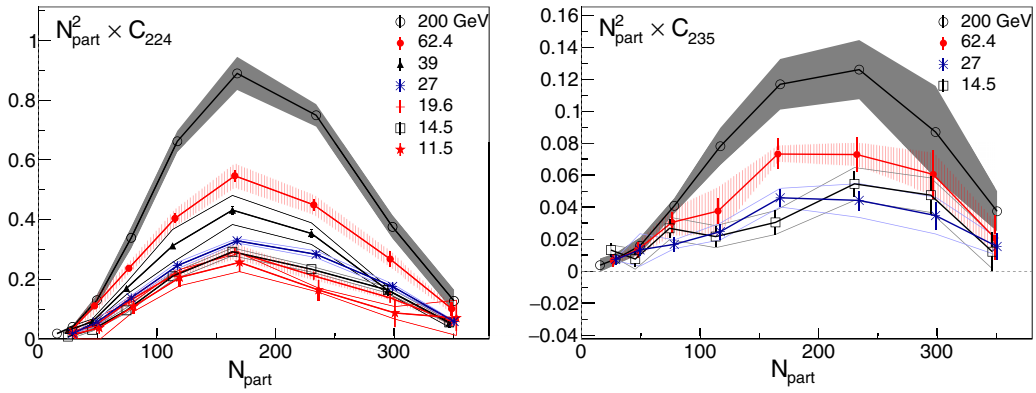

FIG. 12. The centrality dependence of $C_{2,2,4}$ (left) and $C_{2,3,5}$ (right) scaled by $N^2_{\rm part}$ for a selection of energies.

almond-shaped overlap region. A high-density fluctuation in the lower half of the almond zone naturally leads to particles moving upward and away from that density fluctuation so that they both end up in the upper hemisphere. This response was described in Ref. [22] and was illustrated as "Position B" in Fig. 5 of that reference. For energies below 200 GeV, $C_{1,2,3}$ changes sign so that $\langle\cos(\phi'_1+\phi'_2)\rangle$ and $\langle\cos(1\phi'_1-3\phi'_2)\rangle$ are both negative while $\langle\cos(2\phi'_1-4\phi'_2)\rangle$ and $\langle\cos(3\phi'_1-5\phi'_2)\rangle$ are both positive. This condition does not match any of the scenarios in the table but it could indicate an increased preference for particle pairs with $\phi'_1\approx 0$ and $\phi'_2\approx\pi$. A preference for back-to-back particle pairs aligned with the reaction plane would be consistent with an increased importance for momentum conservation at lower energies. Momentum conservation naturally leads to a tendency for particles to be emitted with back-to-back azimuth angles [53]. As the beam energy is decreased, the multiplicity decreases and we should expect the effects of momentum conservation to become more prominent (in the case that only two particles are emitted, they must be back to back). The implications of this change in the configuration of two-particle correlations with respect to the reaction plane deserves further theoretical investigation.

The discussion in the above paragraph illustrates how measurements of $C_{m,n,m+n}$ reveal information about two-particle correlations with respect to the reaction plane and we pointed out two specific conclusions based on the p_T- and $\Delta\eta$-integrated measurements. The value of $C_{1,2,3}$ changes sign as a function of centrality, $\Delta\eta$ and p_T suggesting that

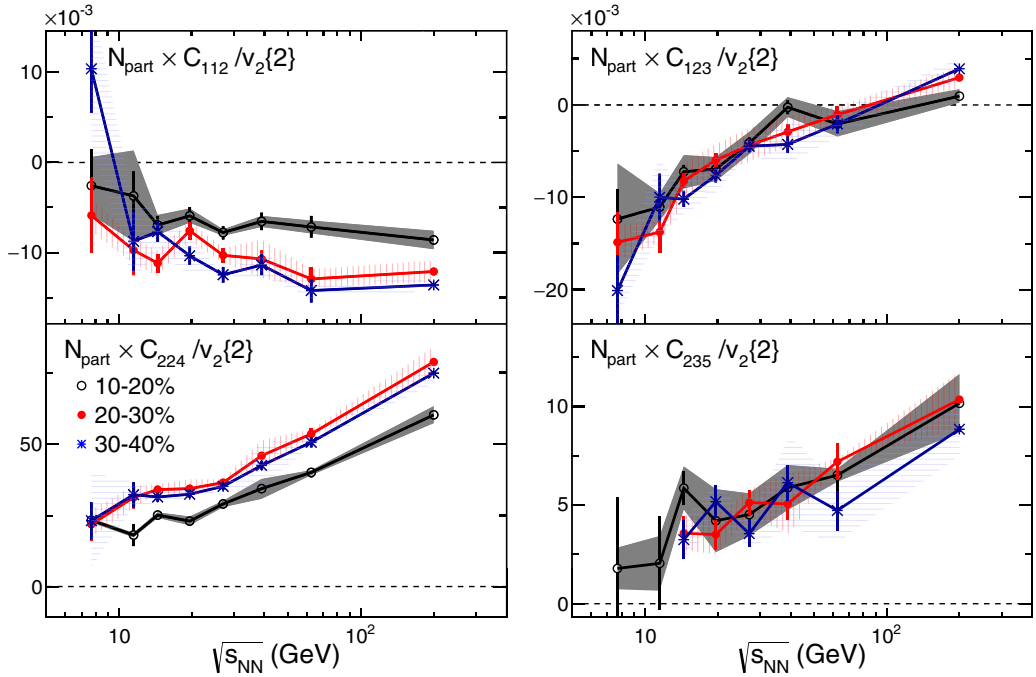

FIG. 13. The $\sqrt{s_{\rm NN}}$ dependence of $N_{\rm part}C_{m,n,m+n}/v_2$ for $(m,n)=(1,1)$ (top left), (1,2) (top right), (2,2) (bottom left) and (2,3) (bottom right) for three selected centrality intervals. In the bottom right panel, the lowest energy points for the 20–30% and 30–40% centrality intervals, having large uncertainties, are omitted for clarity. Statistical uncertainties are shown as vertical error bars while the systematic errors are shown as shaded regions or bands.

TABLE I. Values for $C_{m,n,m+n}/v_2$ for specific cases of ϕ_1' and ϕ_2' where $\phi' = \phi - \Psi_{\rm RP}$ [see Eq. (4)]. The first column ($\phi_1' = \phi_2' = 0$) corresponds to a particle pair with $\Delta\phi = 0$ emitted in the direction of the reaction plane (in-plane). The second column corresponds to back-to-back ($\Delta\phi = \pi$) particles emitted in-plane. The third and fourth columns correspond to pairs of particles emitted perpendicular to the reaction plane (out-of-plane) with either $\Delta\phi = 0$ or $\Delta\phi = \pi$, respectively. The rightmost column is a scenario consistent with the correlations observed in midcentral collisions at $\sqrt{s_{\rm NN}} = 200\,{\rm GeV}$.

	$(\phi_1',\ \phi_2')$ [rad]				
	$(0, 0)$	$(0, \pi)$	$\pm(\frac{\pi}{2}, \frac{\pi}{2})$	$(\frac{\pi}{2}, -\frac{\pi}{2})$	$\pm(\frac{\pi}{3}, \frac{2\pi}{3})$
$C_{1,1,2}/v_2$	$+1$	-1	-1	$+1$	-1
$C_{1,2,3}/v_2$	$+1$	-1	-1	$+1$	$+\frac{1}{2}$
$C_{2,2,4}/v_2$	$+1$	$+1$	-1	-1	$+1$
$C_{2,3,5}/v_2$	$+1$	-1	-1	$+1$	$+\frac{1}{2}$

further specific configurations may arise when triggering on a particular p_T or investigating particles separated by an η gap. We have not examined the charge dependence of $C_{m,n,m+n}$ but future work placing a like-sign or unlike-sign requirement on ϕ_1' and ϕ_2' may be useful for interpreting charge separation measurements and determining whether they should be taken as evidence for the chiral magnetic effect. One caveat of this approach is that we have only used the sign of the correlators, as listed in Table I, to determine the preference of pair emission. Depending on the statistical and systematic uncertainties discussed in this paper, it will be interesting to develop a more robust method by utilizing both the sign and the magnitude of the correlators.

IV. CONCLUSIONS

We presented measurements of the energy, centrality, p_T, and $\Delta\eta$ dependence of three-particle azimuthal correlations $C_{m,n,m+n}$ for a variety of combinations of m and n. We find a strong dependence of $C_{1,1,2}$ on $|\eta_1 - \eta_2|$ and a strong dependence of $C_{1,2,3}$ on $|\eta_1 - \eta_3|$. Meanwhile, $C_{2,2,4}$ and $C_{2,3,5}$ exhibit a smaller but still appreciable dependence on $|\eta_1 - \eta_3|$. This may indicate either the presence of short-range nonflow correlations or a rapidity dependence to the initial energy density signaling a breaking of longitudinal invariance. Simple pictures of nonflow, however, appear to be inconsistent with the overall trends observed in the data. The integrated correlations with $m = 1$ are generally negative or consistent with zero except for $C_{1,2,3}$, which, at 200 GeV, is positive for midcentral collisions while it is negative for all centralities at all of the lower energies. Nonzero values for $C_{1,2,3}$ imply correlations between the second and third harmonic event plane that are predicted from models of the initial overlap geometry. The p_T dependence of the correlations exhibits trends suggesting significant differences between the correlations in peripheral collisions and more central collisions as well as differences for $p_T > 5\ {\rm GeV}/c$ and $p_T < 5\ {\rm GeV}/c$. The quantity $C_{1,2,3}$ as a function of $p_{T,1}$ changes sign as many as three times. While $C_{1,1,2}$ is negative for higher energies, it becomes positive or consistent with zero at 7.7 GeV. By examining the energy dependence of $C_{1,1,2}$, $C_{1,2,3}$, $C_{2,2,4}$, and $C_{2,3,5}$ divided by v_2 we are able to infer that in midcentral collisions at 200 GeV, there is a preference for particle pairs to be emitted with angles relative to the reaction plane of either $\phi_1 \approx \pi/3$ and $\phi_2 \approx 2\pi/3$ or $\phi_1 \approx -\pi/3$ and $\phi_2 \approx -2\pi/3$. At 62.4 GeV and below, this appears to change due to a possible preference for back-to-back pairs ($\phi_1 \approx 0$ and $\phi_2 \approx \pi$) aligned with the reaction plane. It must be noted that such conclusions are based on only the signs of the correlators; a more robust approach utilizing the magnitude of the correlators is left for future studies. These data will be useful for constraining hydrodynamic models [52]. In order to facilitate such future data-model comparisons we also include the measurements of $v_n^2\{2\}, n = 1, 2, 4, 5$, over a wide range of energy, in the Appendix of this paper. Measurements of the charge dependence of the correlations presented here, by revealing information about the preferred directions of correlated particles with respect to the reaction plane, should provide valuable insights into whether or not the charge separation observed in heavy-ion collisions is related to the chiral magnetic effect.

V. SUMMARY

The very first measurement of charge inclusive three-particle azimuthal correlations from the RHIC beam energy scan program, presented in this paper, can provide several new insights into the initial state and transport in heavy-ion collisions. These observables go beyond conventional flow harmonics and provide the most efficient way of studying the correlation between harmonic amplitudes and their phases over a wide range of multiplicities. These observables are well defined and of general interest even when the azimuthal correlations are not dominated by hydrodynamic flow. The major finding of this analysis is the strong relative pseudorapidity ($\Delta\eta$) dependence between the particles associated with different harmonics, observed up to about two units ($\Delta\eta \sim 2$) of separation. Non-flow-based expectations such as fragmentation ($\Delta\eta \sim 1$) or momentum conservation (flat in $\Delta\eta$) can not provide a simple explanation for this result. If the observed correlations are dominated by flow, the current results strongly hint at a breaking of longitudinal invariance of the initial-state geometry at RHIC. The comprehensive study of momentum and centrality dependence of three-particle correlations over a wide range of energy (7.7–200 GeV), presented here, will help reduce the large uncertainties in the transport parameters involved in hydrodynamic modeling of heavy-ion collisions over a wide range of temperature and net-baryon densities. In addition, the charge inclusive three-particle correlations will provide baselines for the measurements of the chiral magnetic effect.

ACKNOWLEDGMENTS

We thank the RHIC Operations Group and RCF at BNL, the NERSC Center at LBNL, and the Open Science Grid consortium for providing resources and support. This work was supported in part by the Office of Nuclear Physics within the U.S. DOE Office of Science, the U.S. National Science

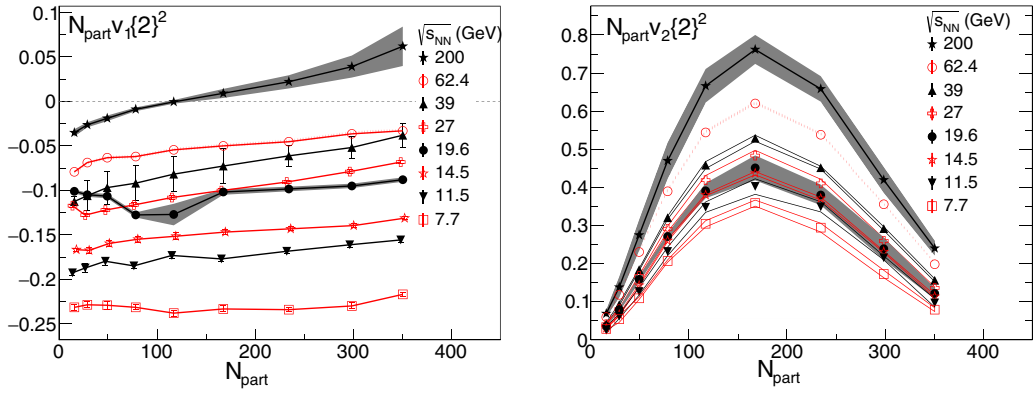

FIG. 14. The $\sqrt{s_{NN}}$ dependence and centrality dependence of $N_{part}v_1^2\{2\}$ (left) and $N_{part}v_2^2\{2\}$ (right) after short-range correlations, predominantly from quantum and Coulomb effects, have been subtracted. For more details see Ref. [18]. The centrality intervals correspond to 0–5%, 5–10%, 10–20%, 20–30%, 30–40%, 40–50%, 50–60%, 60–70%, and 70–80%. The N_{part} values used for the corresponding centralities are 350.6, 298.6, 234.3, 167.6, 117.1, 78.3, 49.3, 28.2, and 15.7 independent of energy.

Foundation, the Ministry of Education and Science of the Russian Federation, National Natural Science Foundation of China, Chinese Academy of Science, the Ministry of Science and Technology of China and the Chinese Ministry of Education, the National Research Foundation of Korea, Czech Science Foundation and Ministry of Education, Youth and Sports of the Czech Republic, Department of Atomic Energy and Department of Science and Technology of the Government of India, the National Science Centre of Poland, the Ministry of Science, Education and Sports of the Republic of Croatia, RosAtom of Russia and German Bundesministerium fur Bildung, Wissenschaft, Forschung and Technologie (BMBF) and the Helmholtz Association.

APPENDIX: TWO-PARTICLE CUMULANTS $v_n^2\{2\}$

In this Appendix we present the measurements of $v_n^2\{2\}$ for $n = 1$, 2, 4, and 5. The second harmonic $v_2^2\{2\}$ was used to scale $C_{m,n,m+n}$ in Fig. 13. Under the assumption that

$$\langle\cos[m\phi_1 + n\phi_2 - (m+n)\phi_3]\rangle \approx \langle v_m v_n v_{m+n}\cos[m\Psi_m + n\Psi_n - (m+n)\Psi_{m+n}]\rangle, \quad \text{(A1)}$$

where Ψ_m is the event-plane angle for harmonic m, one can convert the $C_{m,n,m+n}$ correlations into reaction-plane correlations in the low-resolution limit by dividing by $\sqrt{v_m^2\{2\}v_n^2\{2\}v_{m+n}^2\{2\}}$. The relationship of the $C_{m,n,m+n}$ to v_m and Ψ_m assumes that nonflow correlations are minimal. The analysis of $v_n^2\{2\}$ was performed in a similar manner to that of $v_3^2\{2\}$ presented in Ref. [18]. The $\Delta\eta$ dependence of $\langle\cos 2(\phi_1 - \phi_2)\rangle$ is analyzed for $p_T > 0.2$ GeV/c and $|\eta| < 1$. Short-range correlations are parameterized with a narrow Gaussian peak centered at $\Delta\eta = 0$ and the remaining longer-range correlations are integrated (weighting by the number of pairs at each $\Delta\eta$) to obtain the $\Delta\eta$-integrated $v_n^2\{2\}$ results. The quantity labeled v_2 in Fig. 13 is $\sqrt{v_2^2\{2\}}$.

Figure 14 shows the results for $v_1^2\{2\}$ (left) and $v_2^2\{2\}$ (right) as a function of centrality for 200, 62.4, 39, 27, 19.6, 14.5, 11.5, and 7.7 GeV Au+Au collisions. The data are scaled by N_{part} and plotted verses N_{part} for convenience. At 200 GeV, $v_1^2\{2\}$ is positive for central collisions but becomes negative for $N_{part} < 150$. The negative values are expected from momentum conservation and present a conceptual challenge for dividing $C_{m,n,m+n}$ by $\sqrt{v_1^2\{2\}}$. The values of $v_1^2\{2\}$ become

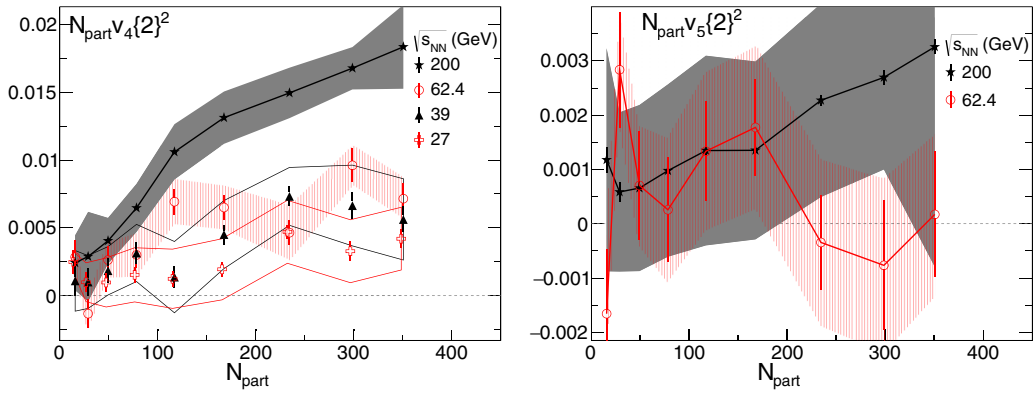

FIG. 15. The $\sqrt{s_{NN}}$ dependence and centrality dependence of $N_{part}v_4^2\{2\}$ (left) and $N_{part}v_5^2\{2\}$ (right) after short-range correlations, predominantly from quantum and Coulomb effects, have been subtracted. For more details see Ref. [18].

more negative at lower energies. This is consistent again with momentum conservation effects, which are expected to become stronger as multiplicity decreases. In the limit of a collision that produces only two particles, momentum conservation would require that $v_1^2\{2\} = -1$. The $v_1^2\{2\}$ results follow a monotonic energy trend except for peripheral collisions at 19.6 GeV, which appear to be elevated with respect to the trends.

The right panel of Fig. 14 shows the results for $N_{\rm part}v_2^2\{2\}$, which remain positive for all energies and collision centralities. While it is unusual to scale $v_2^2\{2\}$ by $N_{\rm part}$, we keep this format for consistency. The scaled results exhibit a strong peak for midcentral collisions due to the elliptic geometry of those collisions.

Figure 15 shows the data for $N_{\rm part}v_4^2\{2\}$ (left) and $N_{\rm part}v_5^2\{2\}$ (right) for a more limited energy range. Results for $N_{\rm part}v_3^2\{2\}$ are available in Ref. [18]. At the lower energies the relative uncertainties on these data become too large to be useful. This result presents another challenge to recasting $C_{m,n,m+n}$ in terms of reaction-plane correlations because scaling by $\sqrt{v_4^2\{2\}}$ or $\sqrt{v_5^2\{2\}}$ leads to a large uncertainty on the resulting ratios.

[1] J. C. Collins and M. J. Perry, Superdense Matter: Neutrons or Asymptotically Free Quarks? Phys. Rev. Lett. **34**, 1353 (1975).

[2] S. A. Chin, Transition to hot quark matter in relativistic heavy ion collision, Phys. Lett. B **78**, 552 (1978).

[3] J. I. Kapusta, Quantum chromodynamics at high temperature, Nucl. Phys. B **148**, 461 (1979).

[4] R. Anishetty, P. Koehler, and L. D. McLerran, Central collisions between heavy nuclei at extremely high-energies: The fragmentation region, Phys. Rev. D **22**, 2793 (1980).

[5] S. Borsanyi *et al.* (Wuppertal-Budapest Collaboration), Is there still any T_c mystery in lattice QCD? Results with physical masses in the continuum limit III, J. High Energy Phys. 09 (2010) 073.

[6] T. Bhattacharya, M. I. Buchoff, N. H. Christ, H. T. Ding, R. Gupta, C. Jung, F. Karsch, Z. Lin, R. D. Mawhinney, G. McGlynn, S. Mukherjee, D. Murphy, P. Petreczky, D. Renfrew, C. Schroeder, R. A. Soltz, P. M. Vranas, and H. Yin (HotQCD Collaboration), QCD Phase Transition with Chiral Quarks and Physical Quark Masses, Phys. Rev. Lett. **113**, 082001 (2014).

[7] Y. Aoki, G. Endrodi, Z. Fodor, S. D. Katz, and K. K. Szabo, The order of the quantum chromodynamics transition predicted by the standard model of particle physics, Nature **443**, 675 (2006).

[8] M. M. Aggarwal *et al.* (STAR Collaboration), An experimental exploration of the QCD phase diagram: The search for the critical point and the onset of De-confinement, arXiv:1007.2613 [nucl-ex].

[9] S. A. Voloshin, A. M. Poskanzer, and R. Snellings, Collective phenomena in non-central nuclear collisions, Landolt-Bornstein **23**, 293 (2010); P. Sorensen, Elliptic flow: A study of space-momentum correlations in relativistic nuclear collisions, Quark-Gluon Plasma **4**, 323 (2010); H. G. Ritter and R. Stock, Collective flow of QCD matter: A Historical introduction, J. Phys. G **41**, 124002 (2014).

[10] J. Adams *et al.* (STAR Collaboration), Minijet deformation and charge-independent angular correlations on momentum subspace (η, ϕ) in Au-Au collisions at $\sqrt{s_{NN}} = 130$ GeV, Phys. Rev. C **73**, 064907 (2006); $\Delta\phi\Delta\eta$ correlations in central Au+Au collisions at $\sqrt{s_{NN}} = 200$ GeV, **75**, 034901 (2007); A. Adare *et al.* (PHENIX Collaboration), Dihadron azimuthal correlations in Au+Au collisions at $\sqrt{s_{NN}} = 200$ GeV, *ibid.* **78**, 014901 (2008); B. I. Abelev *et al.* (STAR Collaboration), Long range rapidity correlations and jet production in high energy nuclear collisions, *ibid.* **80**, 064912 (2009); B. Alver *et al.* (PHOBOS Collaboration), High Transverse Momentum Triggered Correlations Over a Large Pseudorapidity Acceptance in Au+Au Collisions at $\sqrt{s_{NN}} = 200$ GeV, Phys. Rev. Lett. **104**, 062301 (2010); S. Chatrchyan *et al.* (CMS Collaboration), Long-range and short-range dihadron angular correlations in central PbPb collisions at a nucleon-nucleon center of mass energy of 2.76 TeV, J. High Energy Phys. 07 (2011) 076; K. Aamodt *et al.* (ALICE Collaboration), Harmonic decomposition of two-particle angular correlations in Pb-Pb collisions at $\sqrt{s_{NN}} = 2.76$ TeV, Phys. Lett. B **708**, 249 (2012); G. Aad *et al.* (ATLAS Collaboration), Measurement of the azimuthal anisotropy for charged particle production in $\sqrt{s_{NN}} = 2.76$ TeV lead-lead collisions with the ATLAS detector, Phys. Rev. C **86**, 014907 (2012).

[11] S. A. Voloshin, Two particle rapidity, transverse momentum, and azimuthal correlations in relativistic nuclear collisions and transverse radial expansion, Nucl. Phys. A **749**, 287 (2005).

[12] A. P. Mishra, R. K. Mohapatra, P. S. Saumia, and A. M. Srivastava, Super-horizon fluctuations and acoustic oscillations in relativistic heavy-ion collisions, Phys. Rev. C **77**, 064902 (2008).

[13] P. Sorensen, Searching for superhorizon fluctuations in heavy-ion collisions, arXiv:0808.0503 [nucl-ex]; Implications of space-momentum correlations and geometric fluctuations in heavy-ion collisions, J. Phys. G **37**, 094011 (2010).

[14] J. Takahashi, B. M. Tavares, W. L. Qian, R. Andrade, F. Grassi, Y. Hama, T. Kodama, and N. Xu, Topology Studies of Hydrodynamics using Two Particle Correlation Analysis, Phys. Rev. Lett. **103**, 242301 (2009).

[15] P. Sorensen, B. Bolliet, A. Mocsy, Y. Pandit, and N. Pruthi, The rise and fall of the ridge in heavy ion collisions, Phys. Lett. B **705**, 71 (2011).

[16] K. Aamodt *et al.* (ALICE Collaboration), Higher Harmonic Anisotropic Flow Measurements of Charged Particles in Pb-Pb Collisions at $\sqrt{s_{NN}} = 2.76$ TeV, Phys. Rev. Lett. **107**, 032301 (2011); A. Adare *et al.* (PHENIX Collaboration), Measurements of Higher-Order Flow Harmonics in Au+Au Collisions at $\sqrt{s_{NN}} = 200$ GeV, *ibid.* **107**, 252301 (2011); L. Adamczyk *et al.* (STAR Collaboration), Third harmonic flow of charged particles in Au+Au collisions at $\sqrt{s_{NN}} = 200$ GeV, Phys. Rev. C **88**, 014904 (2013).

[17] C. Adler *et al.* (STAR Collaboration), Elliptic flow from two and four particle correlations in Au+Au collisions $\sqrt{s_{NN}} = 130$ GeV, Phys. Rev. C **66**, 034904 (2002).

[18] L. Adamczyk *et al.* (STAR Collaboration), Beam Energy Dependence of the Third Harmonic of Azimuthal Correlations

in Au+Au Collisions at RHIC, Phys. Rev. Lett. **116**, 112302 (2016).
[19] R. S. Bhalerao, J. Y. Ollitrault, and S. Pal, Event-plane correlators, Phys. Rev. C **88**, 024909 (2013).
[20] J. D. Bjorken, Highly relativistic nucleus-nucleus collisions: The central rapidity region, Phys. Rev. D **27**, 140 (1983).
[21] G. Denicol, A. Monnai, and B. Schenke, Moving Forward to Constrain the Shear Viscosity of QCD Matter, Phys. Rev. Lett. **116**, 212301 (2016).
[22] D. Teaney and L. Yan, Triangularity and dipole asymmetry in heavy ion collisions, Phys. Rev. C **83**, 064904 (2011).
[23] Z. Qiu and U. Heinz, Hydrodynamic event-plane correlations in Pb+Pb collisions at $\sqrt{s} = 2.76$ *A*TeV, Phys. Lett. B **717**, 261 (2012).
[24] D. Teaney and L. Yan, Event-plane correlations and hydrodynamic simulations of heavy ion collisions, Phys. Rev. C **90**, 024902 (2014).
[25] H. Niemi, K. J. Eskola, and R. Paatelainen, Event-by-event fluctuations in perturbative QCD + saturation + hydro model: pinning down QCD matter shear viscosity in ultrarelativistic heavy-ion collisions, Phys. Rev. C **93**, 024907 (2018).
[26] S. Ryu, J.-F. Paquet, C. Shen, G. S. Denicol, B. Schenke, S. Jeon, and C. Gale, Importance of the Bulk Viscosity of QCD in Ultrarelativistic Heavy-Ion Collisions, Phys. Rev. Lett. **115**, 132301 (2015).
[27] B. I. Abelev *et al.* (STAR Collaboration), Azimuthal Charged-Particle Correlations and Possible Local Strong Parity Violation, Phys. Rev. Lett. **103**, 251601 (2009).
[28] B. I. Abelev *et al.* (STAR Collaboration), Observation of charge-dependent azimuthal correlations and possible local strong parity violation in heavy ion collisions, Phys. Rev. C **81**, 054908 (2010).
[29] D. Kharzeev, R. D. Pisarski, and M. H. G. Tytgat, Possibility of Spontaneous Parity Violation in Hot QCD, Phys. Rev. Lett. **81**, 512 (1998).
[30] D. Kharzeev, Parity violation in hot QCD: Why it can happen, and how to look for it, Phys. Lett. B **633**, 260 (2006).
[31] S. A. Voloshin, Parity violation in hot QCD: How to detect it, Phys. Rev. C **70**, 057901 (2004).
[32] J. Jia and P. Huo, Forward-backward eccentricity and participant-plane angle fluctuations and their influences on longitudinal dynamics of collective flow, Phys. Rev. C **90**, 034915 (2014).
[33] P. Bozek, W. Broniowski, and J. Moreira, Torqued fireballs in relativistic heavy-ion collisions, Phys. Rev. C **83**, 034911 (2011).
[34] L. G. Pang, H. Petersen, G. Y. Qin, V. Roy, and X. N. Wang, Decorrelation of anisotropic flow along the longitudinal direction, Eur. Phys. J. A **52**, 97 (2016).
[35] C. Shen and B. Schenke, Dynamical initial-state model for relativistic heavy-ion collisions, Phys. Rev. C **97**, 024907 (2018).
[36] N. Borghini, P. M. Dinh, J. Y. Ollitrault, A. M. Poskanzer, and S. A. Voloshin, Effects of momentum conservation on the analysis of anisotropic flow, Phys. Rev. C **66**, 014901 (2002).
[37] A. Bzdak, V. Koch, and J. Liao, Azimuthal correlations from transverse momentum conservation and possible local parity violation, Phys. Rev. C **83**, 014905 (2011).
[38] J. Jia and S. Mohapatra, A method for studying initial geometry fluctuations via event plane correlations in heavy ion collisions, Eur. Phys. J. C **73**, 2510 (2013).
[39] K. H. Ackermann *et al.* (STAR Collaboration), STAR detector overview, Nucl. Instr. Meth. A **499**, 624 (2003).
[40] B. I. Abelev *et al.* (STAR Collaboration), Systematic measurements of identified particle spectra in pp, d^+ Au and Au+Au, collisions from STAR, Phys. Rev. C **79**, 034909 (2009).
[41] A. Bilandzic, R. Snellings and S. Voloshin, Flow analysis with cumulants: Direct calculations, Phys. Rev. C **83**, 044913 (2011); A. Bilandzic, C. H. Christensen, K. Gulbrandsen, A. Hansen and Y. Zhou, Generic framework for anisotropic flow analyses with multiparticle azimuthal correlations, *ibid.* **89**, 064904 (2014).
[42] M. L. Miller, K. Reygers, S. J. Sanders, and P. Steinberg, Glauber modeling in high energy nuclear collisions, Ann. Rev. Nucl. Part. Sci. **57**, 205 (2007).
[43] G. Aad *et al.* (ATLAS Collaboration), Measurement of event-plane correlations in $\sqrt{s_{NN}} = 2.76$ TeV lead-lead collisions with the ATLAS detector, Phys. Rev. C **90**, 024905 (2014).
[44] M. Luzum and J. Y. Ollitrault, Eliminating experimental bias in anisotropic-flow measurements of high-energy nuclear collisions, Phys. Rev. C **87**, 044907 (2013).
[45] M. A. Lisa, S. Pratt, R. Soltz, and U. Wiedemann, Femtoscopy in relativistic heavy ion collisions, Ann. Rev. Nucl. Part. Sci. **55**, 357 (2005).
[46] Q. Y. Shou, Y. G. Ma, P. Sorensen, A. H. Tang, F. Videbæk and H. Wang, Parameterization of deformed nuclei for glauber modeling in relativistic heavy ion collisions, Phys. Lett. B **749**, 215 (2015).
[47] D. Teaney and L. Yan, Non linearities in the harmonic spectrum of heavy ion collisions with ideal and viscous hydrodynamics, Phys. Rev. C **86**, 044908 (2012).
[48] (STAR Collaboration), Proposal for STAR TPC Inner Sector Upgrade (iTPC), STAR Note 0619: https://drupal.star.bnl.gov/STAR/starnotes/public/sn0619.
[49] K. H. Ackermann *et al.* (STAR Collaboration), Elliptic Flow in Au+Au Collisions at $\sqrt{s_{NN}} = 130$ GeV, Phys. Rev. Lett. **86**, 402 (2001); J. Adams *et al.* (STAR Collaboration), Particle Type Dependence of Azimuthal Anisotropy and Nuclear Modification of Particle Production in Au+Au Collisions at $\sqrt{s_{NN}} = 200$ GeV, *ibid.* **92**, 052302 (2004); Azimuthal anisotropy in Au+Au collisions at $\sqrt{s_{NN}} = 200$ GeV, Phys. Rev. C **72**, 014904 (2005).
[50] D. Molnar, Novel mechanism of high-p_T production from an opaque quark-gluon plasma, arXiv:nucl-th/0503051.
[51] L. Adamczyk *et al.* (STAR Collaboration), Beam-Energy Dependence of Charge Separation along the Magnetic Field in Au+Au Collisions at RHIC, Phys. Rev. Lett. **113**, 052302 (2014).
[52] L. Adamczyk *et al.* (STAR Collaboration), Constraining the initial conditions and temperature dependent transport with three-particle correlations in Au+Au collisions, arXiv:1701.06497 [nucl-ex].
[53] L. Adamczyk *et al.* (STAR Collaboration), Fluctuations of charge separation perpendicular to the event plane and local parity violation in $\sqrt{s_{NN}} = 200$ GeV Au+Au collisions at the BNL Relativistic Heavy Ion Collider, Phys. Rev. C **88**, 064911 (2013).